LAWRENCE
LIVERMORE
NATIONAL
LABORATORY

LLNL-JRNL-403361

Atomic Structure and Phase Transformations in Pu Alloys

A. J. Schwartz, H. Cynn, K. J. M. Blobaum, M. A. Wall, K. T. Moore, W. J. Evans, D. L. Farber, J. R. Jeffries, T. B. Massalski

April 30, 2008

Progress in Materials Science

Disclaimer

LLNL-JRNL-403361

Atomic structure and phase transformations in Pu alloys

A.J. Schwartz[a,*], H. Cynn[a], K.J.M. Blobaum[a], M.A. Wall[a], K.T. Moore[a], W.J. Evans[a], D.L. Farber[a], J.R. Jeffries[a], and T.B. Massalski[b]

[a]*Lawrence Livermore National Laboratory, Livermore, CA 94550, USA*
[b]*Carnegie Mellon University, Pittsburgh, PA 15213, USA*

Number of manuscript folios: 1 file, 52 pages
Number of figures: 23
Number of tables: 2
Short running title: Atomic structure and phase transformations in Pu alloys

[*]To whom correspondence should be addressed.
E-mail: schwartz6@llnl.gov
Phone: 1-925-423-3454
Fax: 1-925-423-2451
Adam J. Schwartz
Lawrence Livermore National Laboratory
L-041, 7000 East Avenue
Livermore, CA 94550, USA

Abstract

Plutonium and plutonium-based alloys containing Al or Ga exhibit numerous phases with crystal structures ranging from simple monoclinic to face-centered cubic. Only recently, however, has there been increased convergence in the actinides community on the details of the equilibrium form of the phase diagrams. Practically speaking, while the phase diagrams that represent the stability of the fcc δ-phase field at room temperature are generally applicable, it is also recognized that Pu and its alloys are never truly in thermodynamic equilibrium because of self-irradiation effects, primarily from the alpha decay of Pu isotopes. This article covers past and current research on several properties of Pu and Pu-(Al or Ga) alloys and their connections to the crystal structure and the microstructure. We review the consequences of radioactive decay, the recent advances in understanding the electronic structure, the current research on phase transformations and their relations to phase diagrams and phase stability, the nature of the isothermal martensitic $\delta \rightarrow \alpha'$ transformation, and the pressure-induced transformations in the δ-phase alloys. New data are also presented on the structures and phase transformations observed in these materials following the application of pressure, including the formation of transition phases.

Keywords: Plutonium; Pu–Ga alloys; Phase transformations; Martensitic phase transformations, Pressure-induced transformations, Phase stability

Contents

1. Introduction

Professor Frank Nabarro appreciated very well the challenges and the opportunities that studies of alloy properties contribute to the understanding of the behavior of materials in general, and newly discovered materials in particular. He was particularly interested in the modes of deformation and phase transformations in metals and alloys as they impact the behavior of lattice dislocations and imperfections in the microstructure and thus affect mechanical properties. The current interest in similar aspects of the actinide elements and their alloys fits very well into this picture.

Building upon an enormous collection of knowledge, based on earlier works regarding metallurgical and condensed-matter physics understanding of materials, the actinides community is now beginning to connect the electronic structure to the microstructure, the physical properties, and the mechanical properties. These actinide materials have particularly fascinating and interrelated electronic and structural properties. The knowledge of the electronic structure, crystal structures, phase transformations and phase stability, and connections between these features and properties of plutonium and its alloys constitute an important area of research for nuclear energy, nuclear waste storage and disposal, nuclear devices, and basic science.

Conventional wisdom in metallurgical research suggests that the physical and mechanical properties of materials are related to both the crystal structure and to the microstructure. The crystal structure is the realm of physics and thermodynamics; the microstructure can be very complex and is often overlooked, or insufficiently specified, particularly in alloys. Typically, materials consist of numerous grains interlocked together. Grains can have the same crystal structure, where all grains belong to the same phase, or they may have different structures if more than one phase is present. From the phase diagrams, we can determine the basic information about the expected equilibrium constitution of any selected alloy: the number of phases expected to be present, their composition, and their proportion. The understanding about constitution, combined with ideas about the distribution of the phases involved and their scale in the microstructure, produces a major part of the path toward the understanding and prediction of properties.

While the electronic structure, which dictates the crystal structure, has a profound effect on the properties of the actinide elements, the nature of the microstructure and its development – often under conditions that may be far from equilibrium – is of equal importance. Thus, to truly understand these materials one must have a detailed understanding of the physics over an enormous range of length scales from the electronic structure and the related energies at one end, to the constitution and the distribution of phases at the other. In between these end members is a myriad of additional important structural features such as imperfections, grain boundaries, macroscopic and sub-microscopic perturbations of composition (i.e., inhomogeneities) and all kinds of temporary or permanent instabilities or metastabilities. Furthermore, for most materials the development of microstructure and texture is strongly dependent on chemical kinetics during thermomechanical processing and is thus time dependent. Ultimately, the strong influence of chemical kinetics in the transformations of Pu and its alloys means that unlike chemical equilibrium (which, as J.W. Gibbs points out [1], is path independent), the end state of the system is path dependent. Thus, experiments and associated literature originating from various laboratories, where alloy purity and experimental parameters

can be different, may in many cases, appear contradictory or inconsistent. In evaluating the obtained results, one must keep in mind the thermodynamic path (temperature, pressure, stress) a sample and experiment have traversed to arrive at the final state. In the end, the microstructure is a sum-total of all of the above-mentioned components and this illustrates the real complexity and difficulty in developing a predictive capability for understanding actinide material properties.

Plutonium is produced by nuclear reactions when uranium is bombarded with neutrons. The resulting Pu atom is unstable, with its most common isotope, ^{239}Pu having a half-life of approximately 24,700 years. In a nearly opposite manner, Pu can fission when the atom is bombarded with neutrons, giving off more neutrons and significant amounts of energy. With proper understanding and safe handling, this energy can be harnessed for nuclear power and other nuclear applications. From the perspective of nuclear physics there now exists an extensive understanding of the fundamental processes related to nuclear fission. However, the condensed-matter physics and various metallurgical aspects of Pu and other actinide metals and their alloys are still in the process of active development. Progress continues to be made in the understanding of the electronic structure, the crystal structure changes involved in various phase transformations, and how these features change as a function of temperature, time (aging), mechanical deformation, and the application of pressure.

In this overview, we concentrate on the current state of our understanding of the structures, transformations, and metastable features in Pu and Pu-based alloys with an emphasis on pressure-induced phase transformations. We also comment on the electronic structure and phase stability modeling (calculations). First, however, we begin by briefly reviewing some of the unique aspects of these materials that arise as a result of radioactive decay and aging, and how they affect phase stability and phase transformations.

2. Equilibrium, or lack thereof: alpha decay

Although a Pu atom can decay by a number of different mechanisms, it is the α decay of a ^{239}Pu atom, which emits an alpha particle ($^{2+}$He ion) of ~5 MeV and a uranium recoil atom of ~86 keV, that is most prevalent. As the α particle slows along its 10-μm track through the Pu matrix, it attracts two electrons to become a He atom, leading to a helium generation rate of approximately 41 atomic parts per million per year. TRIM (TRansport of Ions in Matter) calculations indicate that the α particles lose most of their kinetic energy via electronic interactions with the neighboring Pu atoms [2]. Nearing the end of the path, the α particle produces vacancy and interstitial defects, called Frenkel pairs, before coming to rest. Positron annihilation data by Howell et al. [3] indicate that the He atom immediately finds an unfilled vacancy. The He-filled vacancy is mobile in the Pu matrix at ambient temperature and diffuses through the lattice until it meets a second He-filled vacancy, thus forming the nucleus of a He bubble [4]. Using transmission electron microscopy (TEM), Rohr and Staudhammer [5] observed He bubbles in a 21-year-old Pu alloy that was annealed at 400 °C for 1 h, and it was inferred that this high-temperature heat treatment allowed for diffusion and migration of the helium atoms, leading to bubble formation inside the crystalline matrix and along grain boundaries. Wolfer [6] has

predicted the formation of He bubbles in naturally aged (not annealed) Pu, but until the TEM study of Schwartz et al. [4] in 2005, no He bubbles had been observed in naturally aged Pu (unannealed, as opposed to the annealed samples characterized in [5]). They observed that as the He atoms migrate and form bubbles, a distribution of He bubbles develops, leading to an average diameter of 1.3 nm and an average number density of about 1 x $10^{17}/cm^3$. These He bubbles have a He-to-vacancy ratio of approximately 2.5 and a mean inter-bubble spacing of 18 nm. Valone et al. [7] recently modeled the stability of helium bubbles with molecular dynamics and showed that the He bubbles are stable (do not dissolve) to temperatures close to the melting point. The ramifications of He bubble formation on the properties of the Pu alloy include a decrease in density and a calculated increase in strength, due predominantly to the pinning of dislocations by the bubbles during mechanical deformation [8].

On the opposite side of the α decay, the 86-keV recoiling uranium atom undergoes a series of high-energy, nearly elastic collisions, which in turn produce secondary collisions and generate a cascade of vacancies and self-interstitial defects. The formation of the cascades occurs rapidly, on the order of 10s to 100s of picoseconds, producing considerable damage to the lattice. However, this is mostly repaired, as shown by recent molecular dynamics calculations by Kubota et al. that reveal extended periods (up to 10s of nanoseconds) of annealing where lattice periodicity is largely regained [9]. Although much of the radiation damage anneals out at room temperature [10], this self-induced irradiation damage has been associated with an increase in the measured lattice parameter [11-15], an increase in resistivity [10,16], an increase in the elastic constants [17], and the potential for void swelling [18].

A significant consequence of the self-irradiation damage and the resultant change in properties is that Pu never reaches thermodynamic equilibrium [19]. What is more, the composition changes as Pu decays, where uranium, helium, and other daughter products accumulate and continuously alter phase stability [11]. The accumulation of lattice damage and the growth of He bubbles increase the strength of the matrix and likely reduce its ductility. For a martensitic phase transformation, as discussed below, the mechanical hardening of the δ-phase matrix due to the He bubbles will affect the Gibbs free energy and the activation barrier for nucleation and growth. Hence, if a volume change accompanies the phase transformation, the self-irradiation is likely to influence aspects of the martensite start temperature (M_s) and the transformation hysteresis on heating and cooling, and also during the application of external pressure. The increase and accumulation of vacancies and interstitials enable radiation-enhanced diffusion and also thermal activation, which may in turn alter the kinetics of phase transformations. Thus, the self-irradiation in Pu causes the free-energy landscape of the metal to forever change, constantly altering phase stability and behavior. Because this change occurs slowly, over decades, centuries, and millennia, the phase diagram published by Ellinger et al. [20] discussed below suffices to describe the "metallurgical" or "working" equilibrium.

3. Phase Diagrams

Since the publication in the literature of the first Pu–Ga phase diagram by Ellinger et al. [20] and until quite recently, there has been an ongoing dispute in the Pu science community regarding details of the equilibrium constitution diagram. Published Pu – Ga and Pu – Al phase diagrams from researchers in the United States and France indicate that the face-centered-cubic δ phase is thermodynamically stable to sub-ambient temperatures for Ga contents between <2 and 9 atomic percent [20-23]. On the other hand, researchers in the former Soviet Union followed a Pu – Al phase diagram first published in 1958 by Bochvar [24], a Pu – Ga phase diagram published in 1975 by Chebotarev et al. [25], and publications by Timofeeva [26-28] that suggested that the δ phase is only metastable at ambient temperatures and, if it were not for exceedingly slow kinetics, would decompose via a eutectoid reaction at about 100 °C to the monoclinic α phase and the tetragonal intermetallic compound Pu_3Al or Pu_3Ga.

Phase diagram calculations published by Adler in 1991 [29] using the thermochemical-based code F.A.C.T. support the Russian phase diagram by predicting a eutectoid transformation. Although the Chebotarev et al. phase diagram showing the eutectoid [25] and the calculation by Adler [29] confirming this feature have been available in the West, it was only after extensive discussions between Hecker and Timofeeva regarding the experimental approach and the publishing of their paper "A Tale of Two Diagrams" in the Los Alamos Science volumes in the year 2000 [30] that an increasing worldwide consensus on the eutectoid decomposition has developed.

In addition to the phase diagram calculations by Adler [29], recent phase diagram simulations by Baskes et al., using a Modified Embedded Atom Method (MEAM) potential within a molecular dynamics simulation [31], and the calculation by Turchi et al. using the CALPHAD program [32,33], predict the eutectoid reaction. These details have been discussed by Massalski and Schwartz [34].

There have been numerous studies over the past five decades of the crystal structures, phase transformation temperatures, and mechanisms of transformations. However, there is still much to be learned about the near-equilibrium behavior of unalloyed and alloyed Pu. If one considers the implication of the third law of thermodynamics, which posits that the entropy (S) should become zero at zero Kelvin, we would expect that all phases with solid solubility should become perfectly ordered stoichiometric compounds, or a mixture of pure elements, or become unstable [35]. Hence, any retained metastable δ phase below the eutectoid temperature will tend toward total instability near 0 K [34]. In practice, the δ phase is in "constrained" metastable form (providing a "working" phase diagram) at temperatures where diffusion is no longer possible, unless it transforms martensitically to another metastable form.

The confirmation of the eutectoid being above the ambient temperature also comes from the systematic trend observed in related Pu systems, particularly with the IIIB elements in the periodic table (Al, Ga, In, and Tl). Although the details above the δ phase are unclear in the phase diagrams shown in Fig. 1, this sequence of diagrams demonstrates the trend of the eutectoid reactions and temperatures as a function of alloying element. The diagrams suggest that the eutectoid temperature, T_e, in Pu–Ga could be even slightly above 100 °C. Another possible experimental confirmation of the eutectoid is from the work of Blobaum et al. [36] on the martensitic transformations in a δ-stabilized Pu – 2.0 at.% Ga alloy. They found that "conditioning treatments" in the α + Pu_3Ga, β + δ, and γ + δ phase fields enhanced the amount of metastable α′ martensite

transformation upon subsequent cooling, but higher-temperature conditioning in the single-phase δ region did not enhance α′ transformation. It was hypothesized that embryos of the second phases (α, β, γ) form during conditioning, and they facilitate α′ nucleation on cooling. If the eutectoid decomposition did not occur and the δ phase was indeed stable at ambient temperatures, conditioning treatments below 125°C should result in the same amount of α′ as the amount formed after conditioning at high temperatures in the δ phase field. This work will be described in more detail in Section 4.5.

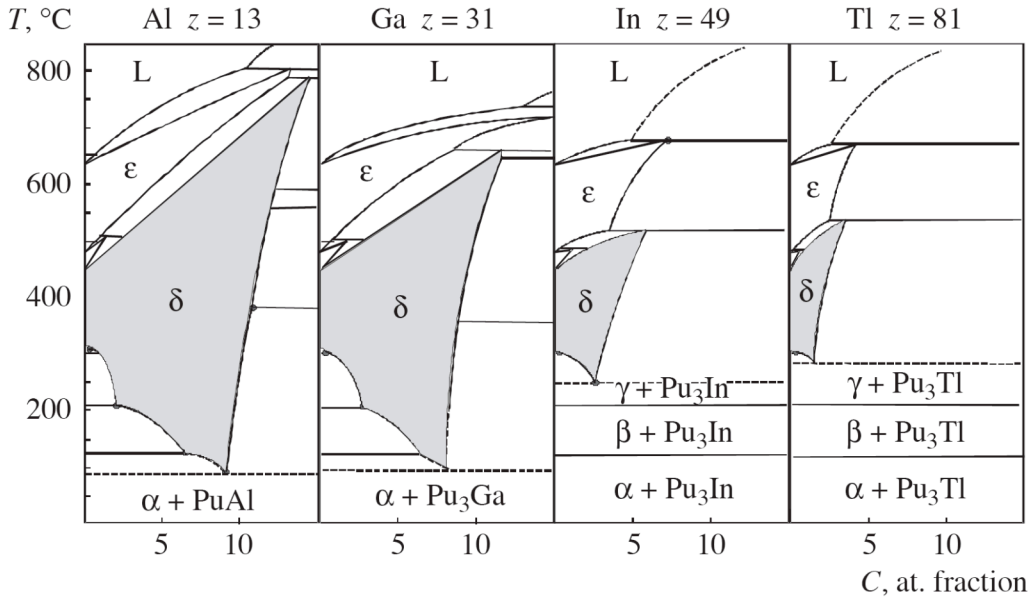

Fig. 1. Proposed phase diagrams of Pu alloys with Al, Ga, In, and Tl (reproduced from [26]) illustrating the influence of alloying element on δ phase stability. Although the details of phase diagram above the δ phase are unclear, the sequence of diagrams demonstrates the trend in the eutectoid temperature with alloying element.

Considering the evidence for a eutectoid decomposition near 100 °C, as discussed above, a modified Pu – Ga phase diagram is proposed in Fig. 2a and compared to the "working" phase diagram in Fig. 2b. These diagrams are based on the phase diagrams published by Hecker and Timofeeva [30], but they have been modified to correct a number of minor inconsistencies concerning the phase rule. The equilibrium diagram (Fig. 2a) indicates a eutectoid transformation to α + Pu_3Ga at approximately 100 °C.

Not shown in Fig. 2 (and other similar published diagrams) are the metastable states. For the case of Pu–Ga alloys with Ga contents between 0.6 and 3.0 atomic percent, the metastable δ phase undergoes a partial transformation at low temperatures to a metastable α′ phase. The "prime" designates the metastable extension of the unalloyed monoclinic α phase with solute trapped in the crystal structure. In other words, if Ga could diffuse out of the monoclinic structure, it would, but is kinetically restricted in a higher energy metastable state. The martensite start temperatures, M_s, and reversion temperatures, R_s, collected from the literature are plotted in Fig. 3.

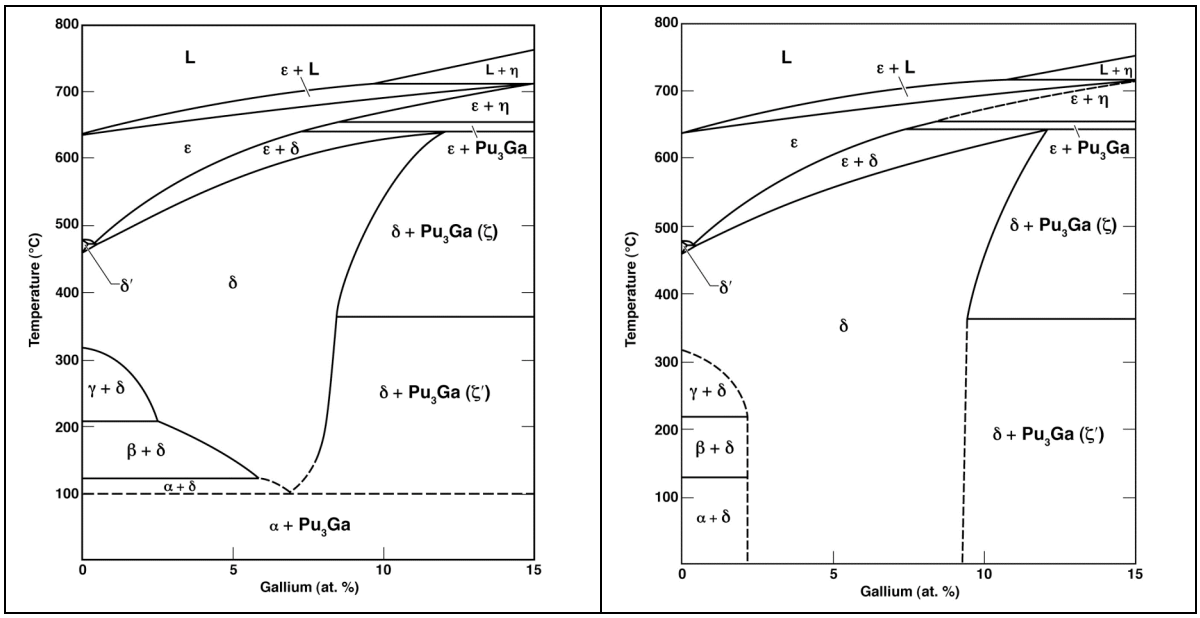

Fig. 2. Pu–Ga phase diagrams. (a) Equilibrium phase diagram with modifications to the diagram published by Hecker and Timofeeva [30], and (b) "Working" phase diagram based on the original work by Ellinger [20].

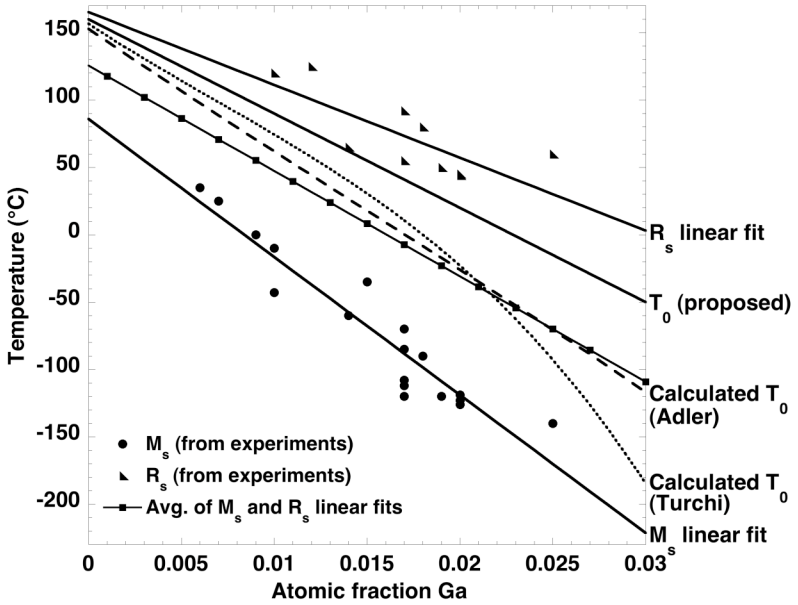

Fig. 3. Calculated $T_o^{\delta/\alpha}$ temperature for the equivalence of free energies between the α and δ phases [29, 32-34]. Also included are the martensite start (δ → α′) and reversion start (α′ → δ) temperatures as a function of Ga content. Note that this is the 5% transformation curve.

The phase diagram calculations by Adler [29] and by Turchi et al. [32,33] also provide the trend in $T_0^{\delta/\alpha}$ (the temperature at which the free energies of the two phases are equal) with increasing Ga content (Fig. 3), as well as the trend with temperature of the (α + δ)/δ phase boundary. It is of interest to keep these trends in mind when constructing the phase diagram itself, and also in order to test how they compare with the experimental

data derived from annealing experiments, the extrapolated portion of the relevant δ phase boundary, or the behavior of the martensitic transformations at low temperatures. The calculation by Turchi et al. [32,33] places the T_0 point for the metastable α/δ transition on the pure Pu axis at 157 °C and this can be used to anchor the proposed trend of the (α + δ)/δ phase boundary inside the phase diagram close to the eutectoid point. Turchi et al. also extended the thermodynamic calculations with calculations of the time-dependent kinetics of the eutectoid decomposition [33]. These calculations are in general agreement with the estimate by Timofeeva [27] and indicate that, below 100 °C, even a small percentage of the eutectoid transformation may take thousands of years.

4. Phase transformations in Pu-based alloys

4.1 General features and nomenclature

The description of the transformation mechanism in a given transformation process may depend on what kinds of atomistic movements are involved. In the words of J.W. Christian [37], "*first-order transformations can be divided into diffusional or displacive. In the diffusional case, atoms move by individual 'jumps' from one structural site to another. There may be some cooperative motion, but in most cases the movements are essentially random.*" Christian refers to such transformations as "civilian." It is well known that diffusional processes are thermally activated. Here, by "thermally activated," we understand that individual atoms, or groups of atoms, will only move when a sufficient thermal energy boost (singly or in cumulative aggregation) has become available from fluctuations. This enables the atoms to escape their original positions within the parent structure to form the new structure. Such a process, therefore, involves two variables: time – waiting for a sufficient agglomeration of fluctuations – and temperature – the magnitude of atomic lattice vibrations. In diffusional transformations, thermal activation occurs during both the nucleation stage and the growth stage of the transformation. Waiting for the formation of a viable nucleus (often referred to as the "critical nucleus") is typically referred to as "incubation time".

In displacive transformations, growth proceeds by a cooperative motion of atoms in a fashion that has been termed "military." Individual atoms move in a way that very much depends on the simultaneous (in step) movement of other adjoining atoms. The extent of the movement of each atom may involve distances corresponding to a fraction of the lattice spacing of either the parent or the product phase, but does not involve long-range diffusion of atoms.

It has become customary to refer to displacive transformations as "martensitic transformations." These transformations also exhibit nucleation and growth features. Three general types of martensitic transformations can be distinguished: athermal, isothermal, and thermoelastic. In athermal martensitic transformations, the amount of the new phase depends mainly on the ease of initial nucleation and the degree of undercooling needed to generate sufficient Gibbs "driving force," i.e., free energy difference between phases. Typically, the opposing stress or strain in the transforming matrix tends to arrest the progress of the transformation. On a typical time-temperature-transformation (T-T-T) diagram, the onset of an athermal martensitic transformation can be represented by a horizontal line (corresponding to the M_s temperature) parallel to the

time axis, i.e., it is independent of time. In athermal martensites, the transformation cannot proceed at a constant temperature because thermal activation alone is not sufficient to bring about additional nucleation, or growth. Further lowering of the temperature results in a reduction of the Gibbs energy and a continuation of the phase transformation.

Isothermal martensite is the product of a displacive phase transformation mode exhibiting thermal activation features. Therefore, incubation times are observed and the amount of martensite formed is a function of both temperature and time. This is in contrast to the athermal martensite, which progresses without thermal activation (i.e., is an a-thermal process) and does not involve incubation times. Isothermal martensitic transformations, like the athermal ones, are also phase changes with a definite change in the crystal structure (therefore this excludes twinning), although, typically, the phase that forms is of lower crystallographic symmetry than the matrix. Because thermal activation is involved during the nucleation stage, the transformation can be represented on a T-T-T diagram in the same way as in diffusional transformations, i.e., as a "C" curve. It is also likely that during the growth stage in isothermal martensites additional nucleation and particle growth can become activated at the same time. Thus, it is the initial fluctuations during the incubation time, the nucleation processes leading to viable particles, and the nucleation and growth of such additional particles that are all thermally activated. None of these require diffusion. In displacive transformations – except for certain situations (i.e., thermoelastic martensites and some isothermal martensites) – the growth process immediately following nucleation is rapid and is typically thought to proceed in the matrix at nearly the speed of sound. Recently, Laughlin et al. [38] discussed the classification of martensites and suggested that the term "isothermal martensite" be replaced with "thermally activated martensite."

Thermoelastic martensites are a special case, where the stresses and strains in the transforming matrix due to the formation of the new phase grains are relatively small. Here, any small change of temperature or external stress can provide sufficient driving force to induce extra growth of the existing new grains. It is possible that a thermoelastic feature is also present in athermal and isothermal martensites. However, this is limited by the volume change as the accompanying elastic and plastic effects arrest the progress of the thermoelastic transformation mode almost immediately.

For Pu-based alloys (and in many other alloy systems), studies of martensitic transformations are typically conducted by thermal cycling. The experiment begins at an ambient temperature followed by a continuous decrease in temperature to the cryogenic range. During cooling, the $\delta \rightarrow \alpha'$ transformation occurs over an extended temperature span. The transformation likely continues if the sample is held isothermally; in some cases additional transformation is observed during heating through the cryogenic range because the matrix is somewhat relieved of accumulated stresses and can thus accommodate more of the martensitic phase. The thermal cycle may continue with a heating portion to observe the $\alpha' \rightarrow \delta$ reversion. During continuous cooling, the incubation times for the initiation of the isothermal transformation accumulate cumulatively until the onset of the transformation is finally detected with *in situ* techniques such as resistivity, differential scanning calorimetry, or dilatometry. Orme et al. [39] first showed that the transformation corresponds to isothermal martensite by observing that the transformation continues in the cryogenic range if the rapid cooling is

arrested and the temperature is held constant. However, the term "isothermal" used to describe the martensitic product resulting from continuous cooling is not strictly correct and this terminology can lead to confusion. Similarly, the reversal of the transformation during heating occurs cumulatively as the temperature rises and has been observed to involve avalanches of reversal bursts leading to distinctive spikes, or steps, in the experimental data (see Section 4.7 below).

Goldberg and Massalski [40] and Hecker, Harbur, and Zocco [41] provided detailed reviews of Pu-based transformations. Schwartz [42] recently discussed a number of outstanding challenges to our understanding of Pu-based alloys. In this review, we update the current understanding of the isothermal martensitic transformation and review in detail the structure and phase transformations in Pu alloys under pressure. We delve into past experiments with the Pu–Al and Pu–Ga alloys, describe new data on the lattice distortions accompanying the transformations, and demonstrate the presence of an intermediate phase (as characterized by x-ray diffraction at a synchrotron facility) that occurs during low-pressure experiments in a diamond anvil cell. In addition, we report on the recovery and transmission electron microscopy, optical microscopy, and x-ray diffraction examination of pressure-induced martensite in Pu–Ga alloys, achieved via a large-volume moissanite anvil cell. Heretofore, the recovery and characterization of specimens subjected to a pressure-induced transformation have been a largely ignored area of research in the literature. Finally, we compare these results with those recently reported by Harbur [43], who proposed the presence of an amorphous phase formed under the application of pressure.

4.2 Previous Results

As stated earlier, a well-homogenized Pu – 2 at.% Ga alloy can be retained in the metastable face-centered-cubic δ phase at room temperature. Ultimately, according to the currently accepted phase diagram in Fig. 2a, this metastable δ phase will decompose at ambient temperatures via a eutectoid transformation to the thermodynamically stable monoclinic α phase and the intermetallic compound Pu_3Ga over a period of approximately 10,000 years [27]. In addition, these low-solute-containing δ phase Pu alloys are metastable with respect to a displacive transformation to the metastable α′ phase either during low temperature excursions [39,44-55] or with the application of stress or pressure [41,43,49,50,56-60].

Using a quench and hold technique, Faiers et al. [46] and Orme et al. [39] demonstrated that the retained δ phase partially transforms to the α′ phase at sub-ambient (cryogenic) temperatures via an isothermal martensitic mode. The observation that the martensite start (M_s) temperature is a strong function of the Ga content was reported by Faires et al. [46], Orme et al. [39], Deloffre et al. [49,50], Hecker et al. [41], and Joel et al. [45]. Adler and Olson reported that the M_s temperature decreases with decreasing grain size [61]. Massalski and Schwartz [34] collected data from the literature that indicate a linear dependence of martensite start temperature as a function of Ga content as shown in Fig. 3. This linear dependence differs from the plot of M_s temperature as a function of the Ga content by Deloffre et al. [49,50] that depicts a kink in the data at 1.5 at.% Ga.

Hecker et al. [41] thoroughly reviewed the literature on phase transformations in Pu–Ga alloys as well as reported for the first time previously unpublished results on the low-temperature and pressure-induced transformations performed at Los Alamos National Laboratory. In both the isothermal martensitic phase transformation and the pressure-induced transformation, they reported a direct transformation from δ to α′, with no evidence of an intermediate phase.

Similar to the Pu–Ga alloy, the low-temperature martensitic phase transformation in high purity, well-homogenized Pu – 2.0 at.% Al alloys occurs directly from the metastable δ phase to the metastable α′ phase, as reported by Hecker et al. in 1981 [47]. The authors use dilatometry to monitor the progress of the transformation and x-ray diffraction to characterize the transformation product upon return to ambient temperature. A M_s temperature of –130 °C is reported and the transformation continues down to liquid nitrogen temperatures. Further transformation is evident in the dilatometry curve upon heating from liquid nitrogen, giving rise to a total volume fraction of α′ phase approximately equal to 25%. Thermal expansion is also evident upon heating, as expected for this composition [44,62]. The transformation is cooling-rate sensitive; a quench to liquid nitrogen temperature in less than 20 seconds is sufficient to suppress the transformation. X-ray diffraction analysis of the α′ phase reveals a significant increase in the lattice parameters relative to the unalloyed α phase, indicating the pronounced effect that Al solutes exert on the bonding in the α′ structure. In addition, the α′ phase exhibits a lower Debye temperature, lower elastic moduli, and a larger coefficient of thermal expansion compared to the unalloyed α phase [41]. The morphology of the α′ particles is highly segmented and resembles lenticular martensites. The authors [47] reported that the reversion from α′ to δ occurs at temperatures lower than the α to β transformation. Interestingly, they also report that for specimens held for more than a year (at ambient and slightly elevated temperatures), the density of the sample increases and the lattice parameters shift toward those of the unalloyed α phase. They interpreted this as diffusion of Ga from the α to δ phase; however, it seems unlikely that Ga can achieve long-range diffusion in the δ phase at this low homologous temperature.

4.3 Microstructure and Crystallography

Because of the large volume change and concurrent stress accumulation involved, the low temperature δ → α′ isothermal martensitic phase transformation in a Pu – 2 at.% Ga alloy only proceeds to partial completion, approximately 20%. The resultant α′ particles dispersed within the δ matrix range from ~1 to 100 μm long by 0.5 to 5 μm wide in the sectioning plane, as shown in the optical micrograph in Fig. 4. Due to limited three-dimensional studies of the precipitates, the overall morphology of the martensitic phase is not accurately known. Depending on the third dimension (into Fig. 4), the precipitates could either be plate-, lath-, or even needle-shaped.

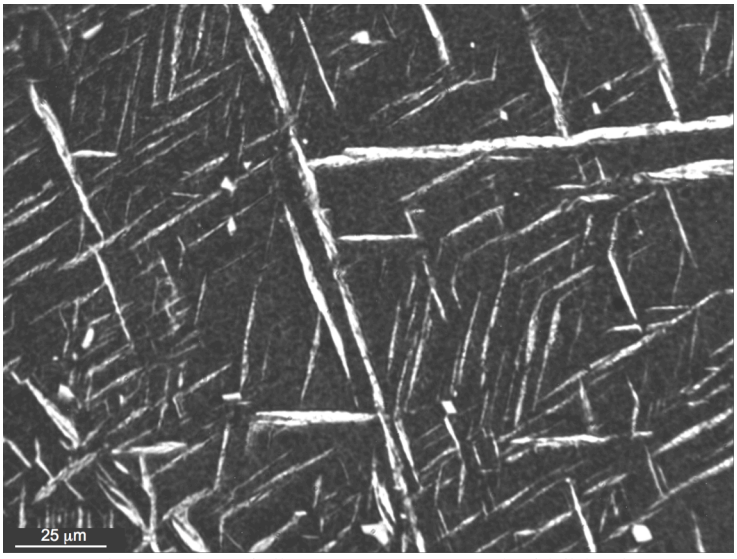

Fig. 4. Optical micrograph of a Pu – 2 at.% Ga alloy, annealed at 375 °C for 8 hours, "conditioned" at 25 °C for 8 hours, and then quenched to –155 °C and held for 4 hours. The α′ particles are the high aspect ratio shapes with light contrast. The δ matrix exhibits dark contrast.

Transmission electron microscopy and electron diffraction investigations by Zocco et al. [48] provide extensive insight into the crystallography and morphology of the $\delta \rightarrow \alpha'$ transformation. The orientation relationship between the α′ particles and the δ matrix is determined to be close to $(111)_{\delta} \parallel (020)_{\alpha'}$ and $[-110]_{\delta} \parallel [100]_{\alpha'}$. Zocco et al. [48] also show $(205)_{\alpha'}$ twinning as an additional lattice invariant deformation mode. Recent work by Moore et al. [53] demonstrates that the orientation relationship is similar to that reported by Zocco et al., but exhibits rotational misalignments of a few degrees between the two phases both parallel and perpendicular to the $[110]_{\delta} \parallel [100]_{\alpha'}$. Moore et al. apply dark-field TEM to the partially transformed two-phase structure and show that the α′ particles consist of two variants rotated 60° around the $<020>_{\alpha'}$ direction as shown in Fig. 5a. High resolution TEM reveals that the α′ / δ interface is composed of a terrace and ledge structure that is faceted on $\{111\}_{\delta}$, in line with the topological model discussed by Hirth et al. [63]. Significant elastic and plastic deformation is required to accommodate the 20% volume decrease during the $\delta \rightarrow \alpha'$ transformation. Krenn et al. [64] and Moore et al. [53] show that the dislocation density increases by nearly two orders of magnitude, from 2.0 x 10^9/cm^2 in an annealed starting material to 2.2 x 10^{10}/cm^2 in a transformed specimen in between α′ particles to 1.7 x 10^{11}/cm^2 near the tip of an α′ particle.

A number of studies beginning with Lomer [65] then Choudhry and Crocker [66], then Adler et al. [67,68], and finally Jin et al. [69] apply theories of martensite crystallography to determine the habit plane of the α′ particles in the δ matrix. Most of these studies predict a $\{123\}_{\delta}$ habit plane with 24 variants, whereas a coupled study of optical metallography and electron diffraction suggests that a significant fraction of the observed habit planes lie on or near the $\{111\}_{\delta}$ [53]. Looking forward, electron backscatter diffraction experiments and additional TEM experiments, including *in situ* heating and cooling experiments, will undoubtedly provide important insights into the transformation crystallography, the habit plane, and other details of the transformation mechanism.

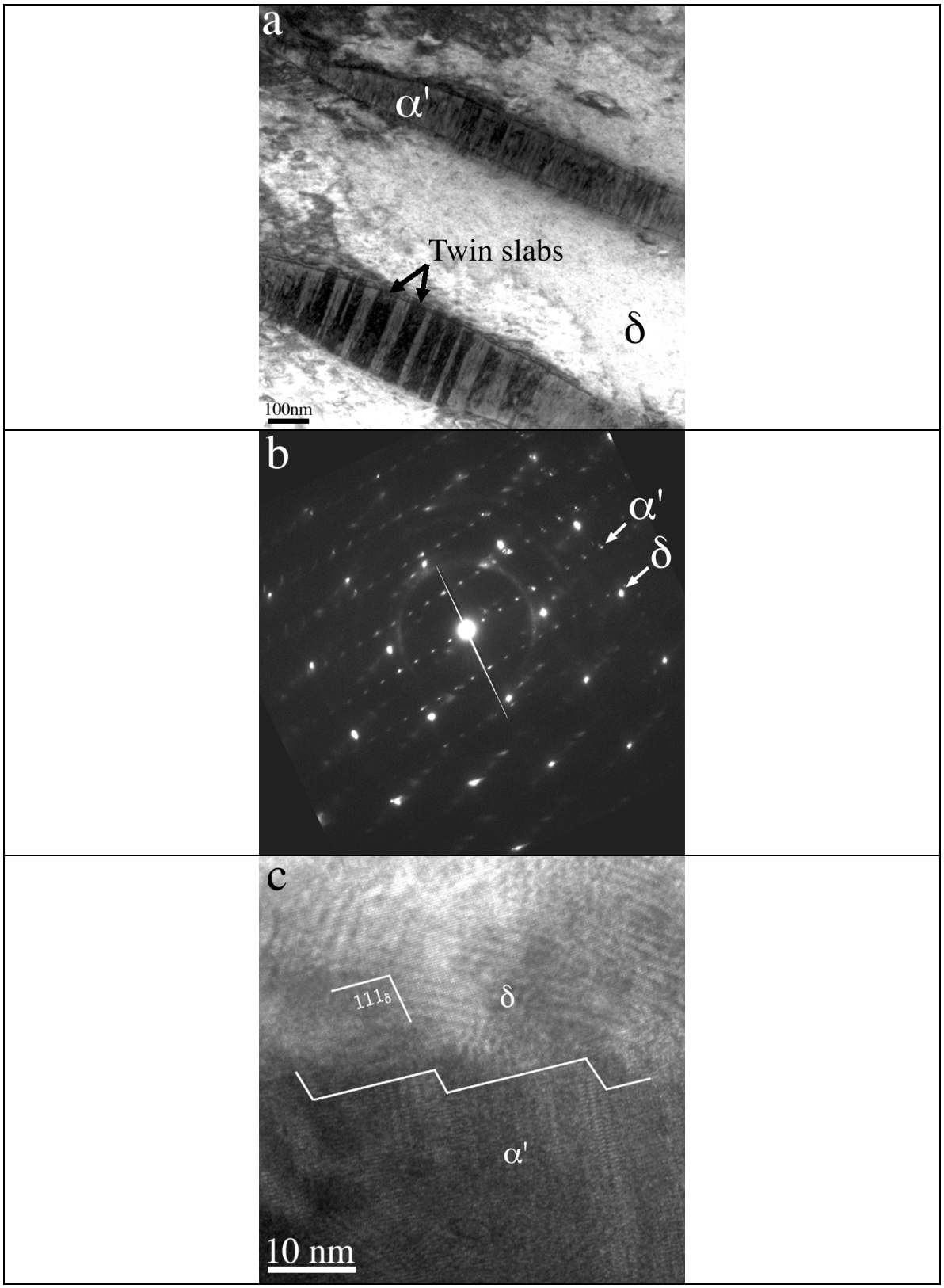

Fig. 5. TEM images and diffraction pattern of the α′ particles in the δ matrix. (a) Bright-field image (b) electron diffraction pattern from the two-phase region, and (c) high-resolution image.

4.4 Double-C curve kinetics

One of the long-standing mysteries in the metallurgy of Pu alloys involves the kinetics of the $\delta \rightarrow \alpha'$ isothermal martensitic transformation as depicted in the experimentally determined time-temperature-transformation (T-T-T) plots [39]. The T-T-T diagrams of Pu – 0.6 at.% Ga and Pu – 0.7 at.% Ga alloys reveal only one C curve, indicative of the balance between driving force and thermal activation that controls the transformation rate, whereas the T-T-T plots of Pu – 1.4 and 1.9 at.% Ga alloys show that there are two overlapping C curves with separate knees. For the Pu – 1.9 at.% Ga alloy in particular, the knee for the upper C is at ~ –130 °C and the knee for the lower C is at ~ –155 °C, as shown in Fig. 6.

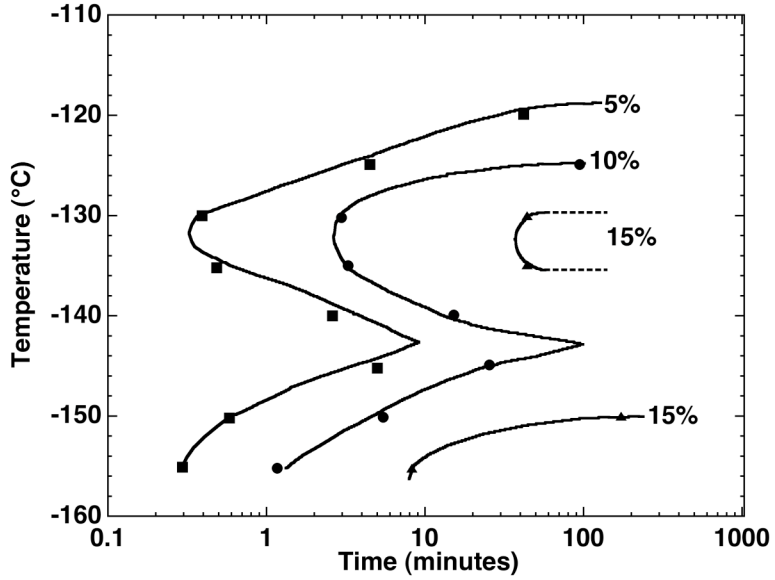

Fig 6. Time-Temperature-Transformation diagram for a Pu – 1.9 at.% Ga alloy (adapted from [39]).

Orme et al. suggest that the transformation in the upper C is a result of a massive transformation, while the lower C results from a martensitic transformation [39]. This interpretation was proposed well before the understanding of massive transformations was developed, and is no longer considered to be a viable possible mechanism for explaining the double C. Since the original Orme et al. publication [39], there has never been any observed microstructure indicative of a massive transformation; there has always been observed a parent-product orientation relationship as demanded by a martensite. Deloffre reports diffusive and displacive components of the transformation and suggests a change in the mechanism that occurs at ~ 1.5 at.% Ga [50], however, details remain unclear. The occurrence of the double C implies the possibility of two distinct thermally activated mechanisms existing for this transformation. Recent differential scanning calorimetry (DSC) work by Oudot et al. [55] adds supporting evidence for the double-C behavior, and reveals a third exothermic reaction above the upper C, as described below in Section 4.6. Differential scanning calorimetry scans on cooling to a sub-ambient isothermal hold temperature reveal three peaks: the first begins at approximately –103 °C, the second at approximately –117 °C, and the third at approximately –131 °C for a Pu – 2.0 at.% Ga alloy. A plot of the area of the reversion

peak (i.e., proportional to the amount of $\delta \rightarrow \alpha'$ reversion) versus isothermal holding temperature reveals two maxima resulting from 18-hour holds at –130 °C and –155 °C. This suggests that the double-C behavior extends to significantly longer times than Orme et al. [39] investigated.

Despite the recently renewed interest to interpret a variety of metallurgical features observed in Pu–Ga alloys, there seems to be as yet no fully satisfactory explanation of the double-C feature in the T-T-T plot associated with the isothermal martensitic transformation in the cryogenic temperature range. Four comments can be made about a possible interpretation:

1) The original suggestion by Orme et al. [39] that the upper portion of the plot may correspond to the onset of a massive transformation should be discarded. There is now sufficient evidence that a massive transformation, while being compositionally invariant, proceeds by a diffusional transfer of atoms at the transformation interface [70]. The occurrence of such transformations at temperatures where the diffusional movement of atoms must be essentially frozen, as in the Pu–Ga case, is therefore exceedingly unlikely. Also, the morphology of the observed transformation, the definitive orientation relationship, and the related crystallographic features are clearly martensitic-like in nature.

2) The recent work by Blobaum et al. [36], discussed in the next subsection on the "conditioning" effects at ambient temperatures, indicates that some pre-nucleation effects can be triggered in the δ matrix at ambient temperatures, which subsequently influence the nucleation and growth behaviors of the α' martensite in the cryogenic temperature range. Recent work by Jeffries et al. [71] also suggests that the double-C plots are strongly influenced by such prior conditioning (often unavoidable because of sample handling). Indeed, as pointed out earlier, the thermodynamic path is critical. Sample "conditioning" plausibly produces nucleation sites with different potencies that require different amounts of thermal activation to trigger the transformation.

3) Deloffre et al. [49,50] have suggested that the observed transformation kinetics could be a manifestation of either a change in the morphology and distribution of the martensitic units that are forming within the δ matrix or a change in transformation path. Indeed, such changes in morphology have been reported by Deloffre et al. [49,50]. These morphological changes may be related to the fact that the driving force for the transformation as well as the elastic stiffness of the matrix are a strong function of the cryogenic temperature to which a sample is cooled. However, why a particular morphology arising from such effects could change into another morphology with temperature, producing the double-C effect, is, at this time, not at all clear. The proposal of an intermediate transformation from $\delta \rightarrow \gamma' \rightarrow \alpha'$ for Ga concentrations below ~1.5 at.% is very intriguing and is quite plausible. Unfortunately, the journal article provided no supporting evidence for this intermediate transformation product.

4) Sadigh and Wolfer proposed a mechanism by which short-range diffusion occurs in the upper C such that Ga atoms migrate to a low-energy, low-volume site in the monoclinic lattice [72]. In the lower C, the temperature is too low to permit this short-range diffusion and thus the Ga atoms remain located at random positions. This hypothesis also appears unlikely because, if this proposal were true, there would be measurable differences in the reversion temperature of the α' particles formed in the upper- and lower-C curves, and this is not observed [55]. In addition, extended x-ray

absorption fine structure experiments by Nelson et al. indicate a random distribution of Ga among all 8 possible lattice sites in the α' phase [73].

Pu–Ga alloys are not the only materials to exhibit two C curves in the T-T-T diagram as a result of an isothermal martensitic phase transformation. An Fe – 17 at.% Cr – 8 at.% Ni alloy was reported to undergo an isothermal martensitic transformation that exhibited two knees while being held above the athermal M_s [74]. Imai et al. showed that initially the transformation in the upper C proceeds from the face-centered-cubic γ phase to the hexagonal-close-packed ε phase. The body-centered-cubic α' phase was observed to grow in at longer times while being held in the temperature range of the upper C. The habit plane of this α' phase was $(111)_\gamma$, whereas the habit plane of the α' that forms directly in the lower C as well as the α' that forms athermally below M_s exhibited a habit plane of $(225)_\gamma$. These results suggest that intermediate transformations and differing habit planes are also possible for the Pu–Ga alloys. Indeed, a sequential phase transformation path in Pu–Ga has been proposed by Lookman et al. [75] where a trigonal and a hexagonal phase separate the fcc and monoclinic phases in the $\delta \rightarrow \alpha'$ transformation.

Although recent experiments and modeling shed further light on the kinetics of the $\delta \rightarrow \alpha'$ transformation, we still do not understand the basic reason for the double-C kinetics. Does it result from different transformation mechanisms, different transformation paths, different morphologies, different embryos or nucleation sites, or something else? How do the kinetics change with age? Further experiments, such as systematic studies of quench and isothermal holds at various temperatures in the double-C plots and *in situ* crystallographic characterization of the phase transformations during cooling and under pressure (proposed in Section 6) are needed. However, due to the toxic and radioactive nature of the materials, simply defining and conducting an experiment is not always feasible. One must approach any given question with the tools at hand, and often this takes some improvisation and creative thinking.

4.5 Effects of conditioning treatment

Blobaum et al. [36] report that the cooling-induced amount of alpha-prime formed in a previously cycled sample depends on how it is "conditioned" subsequent to a high-temperature annealing treatment. That is, the transformation depends on details of the thermal cycling. The observation that a phase transformation could be affected by a low-temperature treatment *after* a high-temperature treatment is unexpected and unusual in metals.

In performing consecutive continuous cooling and heating experiments, Hecker et al. [41] demonstrated that the amount of $\delta \rightarrow \alpha'$ transformation in Pu – 1.8 and 2.0 at.% Ga alloys decreases with each thermal cycle even though it appears that all α' reverts to δ during the heating portion of the cycle. However, Blobaum et al. [36] found that a high-temperature anneal (375 °C) followed by an ambient temperature "conditioning" treatment prior to each thermal cycle produced approximately the same amount of α' in each consecutive cycle. By using the prescribed annealing and conditioning sequence, a single Pu–Ga sample has been thermally cycled 60+ times. Although significant grain growth occurs through the course of these thermal cycles, the authors did not observe systematic changes in transformation behavior (e.g., M_s temperature, R_s temperature, and

amount of transformation). In fact, "control" runs through the course of the experiment give highly reproducible results from cycle to cycle. It should be noted that Adler and Olson [61] showed that M_s was a function of grain size below approximately 150 μm, but this behavior was not observed by Blobaum et al. for grain sizes above ~50 μm. However, no details of a possible inadvertent conditioning treatment following the thermal treatments were described by Adler.

It has been proposed that during the 25 °C conditioning treatment, which is in the α + Pu_3Ga phase field of the equilibrium phase diagram in Fig. 2a, embryos of the thermodynamically stable α phase form isothermally. Upon cooling, these embryos nucleate α′ particles. Without the conditioning treatment, only a small amount of α′ forms on cooling, and it is hypothesized that these particles nucleate on "intrinsic" sites such as grain boundaries, impurities, and dislocations.

Using differential scanning calorimetry (DSC), Blobaum et al. showed the effects of conditioning time on the δ → α′ transformation in a Pu-2.0 at.% Ga alloy. Fig. 7 shows the cooling (Fig. 7a) and heating (Fig. 7b) portions of the DSC scans following conditioning treatments between 0 and 12 hours (in each case, the sample was annealed at 375 °C for 8 hours before conditioning). The areas of the δ → α′ and α′ → δ peaks increase with length of the conditioning treatment, until they saturate at approximately 6 hours. Additional conditioning time, up to 72 hours, did not result in additional α′ formation upon subsequent cooling (Fig. 8). Although the fundamental mechanism or mechanisms that control the timescale of the conditioning treatment is not yet fully understood, it is not surprising that the amount of α′ reaches a plateau. It is well known that the δ → α′ transformation does not go to completion; stress accumulation in the δ matrix due to the 25% volume contraction between the δ and α′ phases is likely to prevent complete transformation, as indicated by the finite-element method analysis described in Krenn et al. [64] and Moore et al. [53].

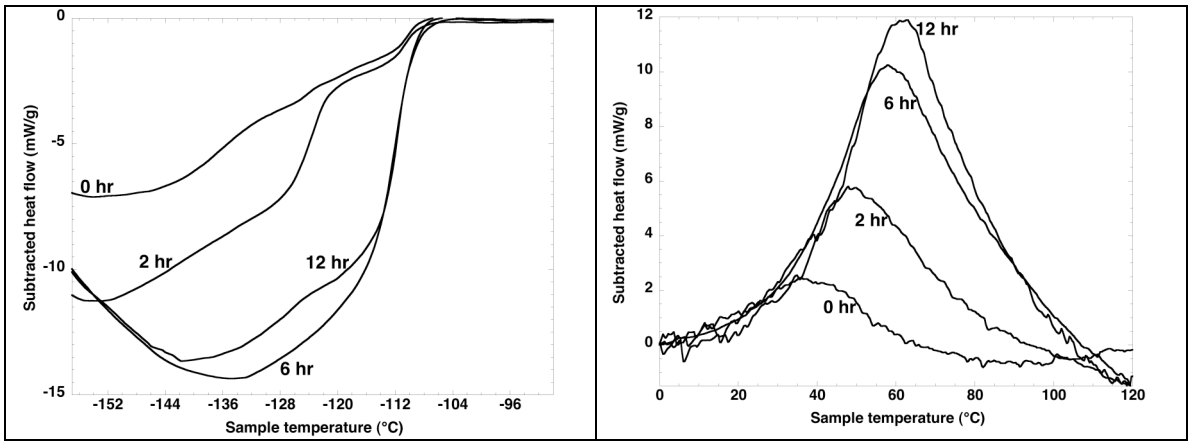

Fig. 7. Differential scanning calorimetry scans (at 20 °C/min) of a Pu – 2.0 at.% Ga alloy that was conditioned at 25 °C for 0 – 12 hours. Peak areas for both the δ → α′ transformation on cooling (a) and the α′ → δ reversion on heating (b) increase as the conditioning time increases, with a plateau at approximately 6 hours.

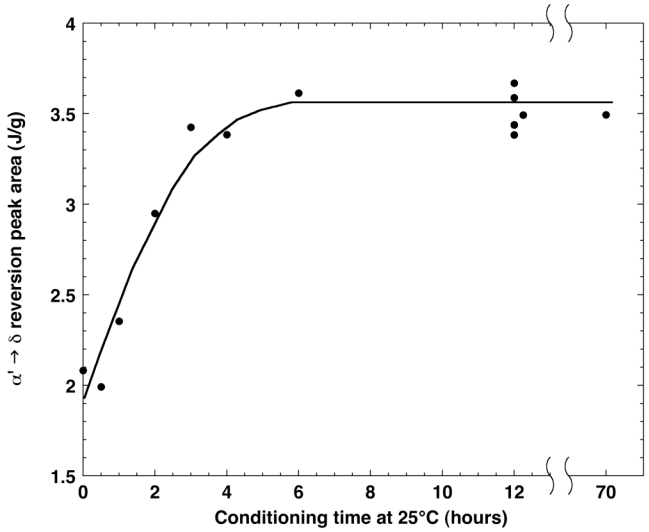

Fig. 8. The amount of δ → α′ transformation on cooling as a function of conditioning time at 25 °C. The amount of transformation product increases rapidly as a result of the first 4 hours of conditioning. No additional transformation on cooling is observed for conditioning treatments of 6 hours or longer.

Blobaum et al. also considered the effect of conditioning *temperature* on the amount of α′ formation. Figure 9 shows cooling (a) and heating (b) portions of DSC thermal cycles following 3 to 16 hour conditioning treatments at temperatures ranging from –50 °C to 370 °C. In each case, the conditioning treatment follows an 8-hour anneal at 375 °C. The largest amount of transformation and reversion occurs following conditioning treatments at 25 °C. Conditioning treatments at –50 °C and 370 °C result in approximately the same amount of α′ formation as when a conditioning treatment is not performed.

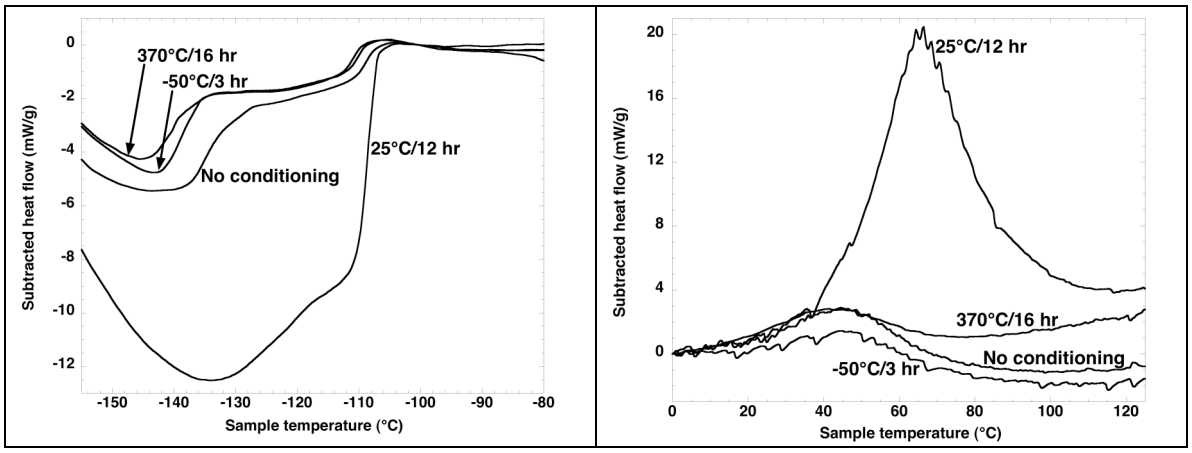

Fig. 9. Differential scanning calorimetry scans (at 20 °C/min) of a Pu – 2.0 at.% Ga alloy that was conditioned at temperatures between -50 °C and 370 °C. (a) Cooling curve and (b) heating curve. The largest amount of α′ is formed when the sampled is conditioned for 12 hours at 25 °C.

Recent work by Jeffries et al. [76] on a well-homogenized (460 °C for 534 hours) Pu – 2.0 at.% Ga alloy confirms that conditioning temperatures between 25 and 50 °C result in the largest amount of δ → α′ transformation (Fig. 10). Conditioning treatments at 0 °C

and 75 °C resulted in less α′ formation than the conditioning treatments at 25 and 50 °C, albeit the amount of transformation is only slightly less. Based on this work, they conclude that homogenization does not influence the conditioning treatment.

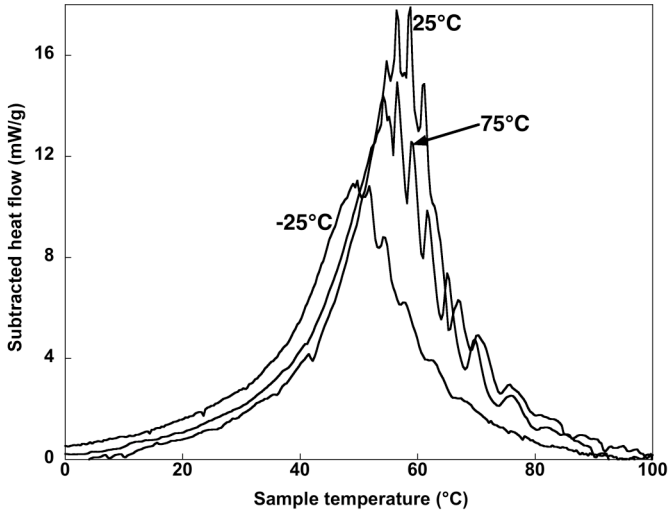

Fig. 10. Differential scanning calorimetry scans (heating at 20 °C/min) of the α′ → δ reversion in a well-homogenized Pu – 2.0 at.% Ga alloy. Prior to the δ → α′ transformation on cooling (not shown), the sample was annealed at 375 °C for 8 hours and then conditioned at the temperatures indicated on the graph for 8 hours.

Blobaum et al. [36] hypothesize the conditioning treatment allows embryos of the equilibrium α phase to form diffusively, and, upon cooling, these embryos nucleate α′ particles. The optimal temperature for formation of α embryos is the result of a competition between higher driving force (larger undercooling) at low temperatures and higher thermal activation at high temperatures. Based on the experiments described here, temperatures between 25 and 50 °C provide the optimal balance for the formation of α embryos. While other second phase-embryos (i.e., β or γ) may also serve as nucleation sites for α′ upon cooling, Fig. 9 indicates that they are either less effective or they form more slowly during conditioning.

When the sample is not conditioned, or when it is conditioned in the single δ-phase field (370°C), a small amount of α′ forms on cooling. In these cases, α′ particles likely nucleate on "intrinsic" sites such as dislocations, helium bubbles, and grain boundaries. However, these intrinsic sites have a lower potency compared to α embryos, which is not surprising because the α embryos have the same crystal structure (and similar lattice parameters) as α′.

Although the careful, reproducible studies by Blobaum et al. [36] and Jeffries et al. [76] have highlighted the effects of conditioning, there are still open questions about the hypothesized α′ embryos. First, why have we never observed α embryos with a microscopic technique? It is not clear that they could be distinguished, even with high-resolution TEM, because of their small size or small strain fields. Perhaps a sensitive *in situ* technique, such as electrical resistivity or resonant ultrasound spectroscopy [77], might be used to detect a progressive change that occurs on the order of a few hours. Second, once a sample has been conditioned, what annealing times and temperatures are required to destroy the conditioning effects? Work is currently underway by Jeffries et

al. [76] to resolve this question. Third, as Pu samples age and the number of helium bubbles and vacancies increase, will a conditioning treatment be necessary to maximize α' formation, or will these intrinsic nucleation sites be sufficient? This is still an open question, and it will be enlightening to study old samples that have been conditioned for decades.

4.6 Unknown exothermic reaction

Regardless of the conditioning time and temperature, an exothermic reaction is observed in the DSC when the sample is cooled to approximately –103 °C. This small exothermic peak has been observed in both partially homogenized and well-homogenized Pu – 2.0 at.% Ga alloys, and it reproducibly occurs prior to the major reactions at lower temperatures.

The reason Oudot et al. [55] referred to this exotherm as a precursor rather than the onset of $\delta \rightarrow \alpha'$ transformation is that, in optimally conditioned samples, two additional larger exotherms are observed at lower temperatures (–117 °C and –131 °C). The double-C curve in the T-T-T diagram suggests that two exotherms should be observed during cooling, with each exotherm signaling the onset of the transformation. Although the onset temperatures for these two exotherms are higher than the knees in the T-T-T plots for this alloy (–131 °C and –155 °C), these exotherms were observed on continuous cooling, while the knees were determined from isothermal holds and represent maximum transformation rates. Given the shape of the C-curve, it is reasonable that the onset of transformation, as observed with continuous cooling experiments, occurs at a higher temperature than the knee of the C-curve. Furthermore, the lower-C curve is expected to extend into the upper-C curve at long times, and therefore, the onset temperature for the second exotherm could be even higher than the knee for the upper-C curve, if cooling rates are sufficiently slow. As with the origin of the double C, the origin of the small initial exothermic reaction remains an unknown.

4.7 Burst martensite

The $\delta \rightarrow \alpha'$ transformation and corresponding $\alpha' \rightarrow \delta$ reversion occur via a burst martensitic mode [51,52]. In this mode, nucleation or initiation of the transformation occurs slowly compared to the growth, which occurs in a "burst." For the forward transformation, nucleation of α' in the δ matrix is required and these nucleation events occur individually as a stochastic process. As each nucleus reaches a critical size, it bursts to its final size. For the reversion, however, the presence of residual δ phase, renders nucleation unnecessary, and the δ/α' interface simply moves to consume the α' particles. When an α' particle reverts, it leaves regions of stress that can either facilitate or hinder reversion of additional adjacent particles [64], which leads to avalanches or cascades of groups of α' particles reverting nearly simultaneously in a cooperative process. These avalanches have been observed as spikes in DSC data (and as steps in dilatometry and electrical resistivity data) from samples that were thermally cycled at constant rates and held isothermally at constant temperatures.

Figure 11 (a) and (b) show DSC data from the $\delta \rightarrow \alpha'$ transformation and $\alpha' \rightarrow \delta$ reversion, respectively, in a partially homogenized Pu – 2.0 at.% Ga alloy that was cooled

and heated at 20 °C/min. On cooling, the forward transformation exhibits a smooth exothermic trace with two or more overlapping peaks beginning at approximately –100 °C. Although each martensite particle grows individually, the observed data is the sum total of many of these events occurring simultaneously. This results in a smooth DSC trace. In the raw (no baseline subtracted) data, which is not shown here, one would expect the curve to return to the baseline when the transformation was complete, but we do not observe such behavior here [52]. Instead, the trace that proceeds as an exotherm might continue if the instrument could be cooled further than –160 °C. It is likely that lower temperatures, longer times, or both are required for the maximum amount of α' to form, recognizing that less than 100% of the δ phase transforms to α'.

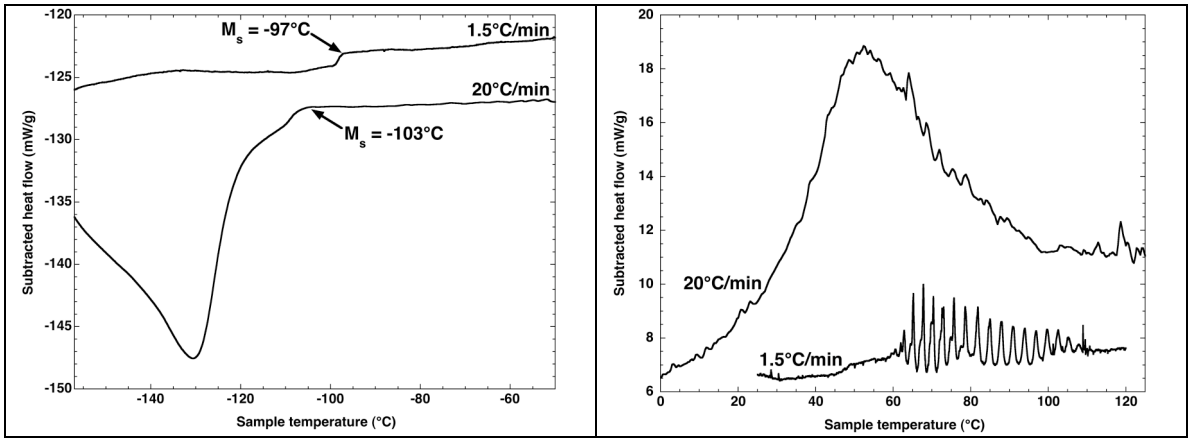

Fig. 11. (a) Cooling portion of DSC scans from a partially homogenized Pu – 2.0 at.% Ga alloy. The exothermic peaks correspond to the $\delta \rightarrow \alpha'$ martensitic transformation. M_s is the martensite start temperature. (b) Heating portion of DSC scans from a partially homogenized Pu – 2.0 at.% Ga alloy. The endothermic peaks correspond to the cooperative $\alpha' \rightarrow \delta$ reversion. Sharp spikes are evident on the high-temperature side of the 20 °C/min scan, and throughout the 1.5 °C/min scan.

The reversion data show a series of periodic endothermic spikes that become more distinct as the heating rate is decreased. Each spike corresponds to a cascade of α' particles reverting to δ and two factors may contribute to quenching each cascade. First, the $\alpha' \rightarrow \delta$ reversion is endothermic and local decreases in temperature may suppress a cascade; new cascades may be initiated as the DSC continues to heat the sample at a constant rate. Second, finite-element modeling indicates that reverted α' particles leave regions of stress in the δ matrix that can enhance or diminish additional reversion, depending on their location along the α' particle [53,64]. As these stress fields accumulate during the cascade, it is likely that the system reaches a point where it does not have sufficient thermal activation energy to overcome the stress and revert additional particles. Further heating by the DSC instrument then initiates the next cascade.

Recently, cooperative $\alpha' \rightarrow \delta$ reversion has been observed in DSC scans of a well-homogenized Pu – 2.0 at.% Ga alloy. Prior to the DSC experiments, the material was annealed at 460 °C for 534 hours. The heating scan at 20 °C/min in Fig. 12 shows spikes on the high temperature side of the $\alpha' \rightarrow \delta$ reversion peak. These spikes are similar to those observed in the partially homogenized Pu – 2.0 at.% Ga alloy (Fig. 11). Therefore, cooperative reversion cascades are a real effect and are not due to inhomogeneous Ga

distribution where reversion of different groups of α′ particles occurs in areas with different gallium concentrations.

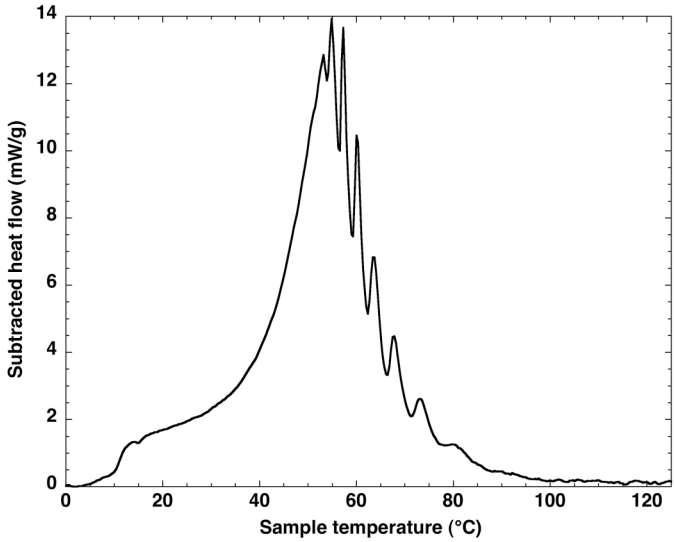

Fig. 12. Heating portion (at 20 °C/min) of a DSC scan from a well-homogenized Pu – 2.0 at.% Ga alloy. Sharp spikes are evident on the high-temperature side of the endothermic α′ → δ reversion peak.

Cooperative α′ → δ reversion cascades are not caused or impeded by the prior conditioning treatment. Fig. 10 shows 20 °C/min DSC heating scans of a well-homogenized Pu – 2.0 at.% Ga alloy that was subjected to 8 hour conditioning treatments (described in Section 4.5) between -25 °C and 100 °C, after annealing at 375 °C for 2 hours. For conditioning treatments between 0 °C and 75 °C, spikes are evident on the high temperature side of the α′ → δ reversion peak, and they are qualitatively similar in each case. For the conditioning treatments at –25 °C and 100 °C, small spikes are distinguishable on the high-temperature side of the peak, but they are not as distinct as they are after the other conditioning treatments. While it might seem reasonable that each reversion cascade corresponds to a group of α′ particles formed from embryos with a certain potency, Fig. 10 indicates that this is not the case. The conditioning treatment does not affect the cooperative reversion behavior.

Cascades of α′ → δ reversion are also observed during isothermal holding in the DSC. A partially transformed Pu – 2.0 at.% Ga alloy was heated at 5 °C/min to 65 °C and held isothermally in the DSC instrument. At 65 °C, the α′ → δ reversion is approximately 50% complete. Figure 13 shows the spikes observed during the hold; one large spike occurs immediately, and several more follow, each a few minutes apart and progressively smaller. Each spike corresponds to a cascade of α′ particles reverting cooperatively to the δ phase. No additional spikes occurred after the small spike at 102 minutes, although the sample was held at 65 °C for an additional 50 minutes. All of the spikes in Fig. 13 have a sharp onset and a more gradual termination, indicating the cascades start abruptly with a large number of particles reverting nearly simultaneously and then the cascade tapers off with fewer particles. The observation of these spikes occurring randomly in time during an isothermal hold has not been reported previously for a martensite transformation. These data indicate that the α′ → δ reversion occurs

isothermally, and the initiation of reversion cascades is a stochastic process, even though nucleation is not required. Each cascade is likely to be triggered by a thermal fluctuation.

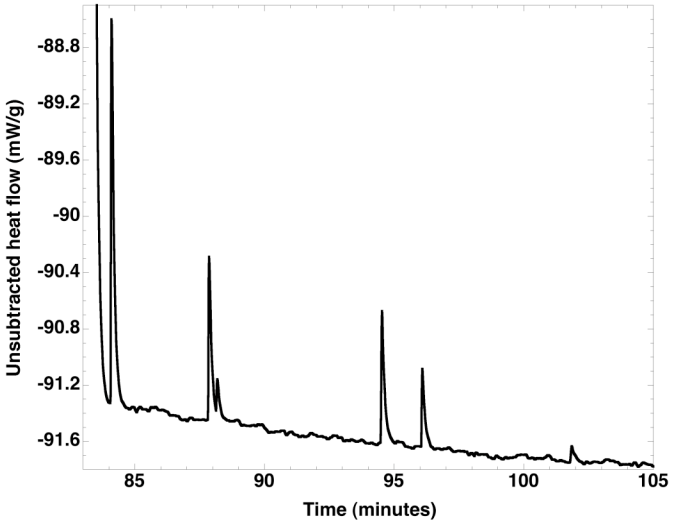

Fig. 13. Differential scanning calorimetry trace showing the isothermal $\alpha' \rightarrow \delta$ reversion at 65 °C in a partially homogenized Pu – 2.0 at.% Ga alloy.

Additional isothermal transformation occurs when the hold temperature is increased. The same Pu – 2.0 at.% Ga alloy was annealed, conditioned, and partially transformed again. This time, it was held isothermally for 45 minutes at progressively higher temperatures ranging from 65 to 105 °C. The data are shown in Fig. 14a. At nearly every temperature, small spikes are observed. At 65 °C, the largest number of spikes occur, and they do not begin until 2.5 minutes after reaching the hold temperature. When the temperature is increased to 70 and 75 °C, the first reversion cascades occur within the first 2 minutes, but there are fewer cascades occurring later in the hold. The largest cascades occur after 14.4 minutes at 90 °C and after 2.8 minutes at 105 °C. After holding for 45 minutes at 105 °C, the sample was heated at 5 °C/min to 350 °C (Fig. 14b). Additional spikes are observed up to 200 °C during the heating, with an initial large spike and extended peak occurring between 110 and 127 °C. This initial peak may correspond to the remainder of the $\alpha' \rightarrow \delta$ reversion, and the successive smaller spikes may correspond to $\alpha \rightarrow \beta$ transformation. This sample was inadvertently annealed in the $\delta + \varepsilon$ phase field where gallium diffusion is very fast, so the sample is likely to have regions of very low gallium at the grain boundaries. Figure 15 shows heating data at 10 °C/min and 20 °C/min for this sample. The stepped isothermal holds indicate that reversion of all the α' particles does not occur at the reversion start temperature, even after long times. These results suggest that stress accumulation in the δ matrix in the form of increased elastic strain and increased dislocation density, due to prior reversion cascades, causes the remaining cascades to have progressively higher activation energies. Thus, stress accumulation is likely to be a larger factor than local temperature decreases in arresting each cooperative reversion cascade.

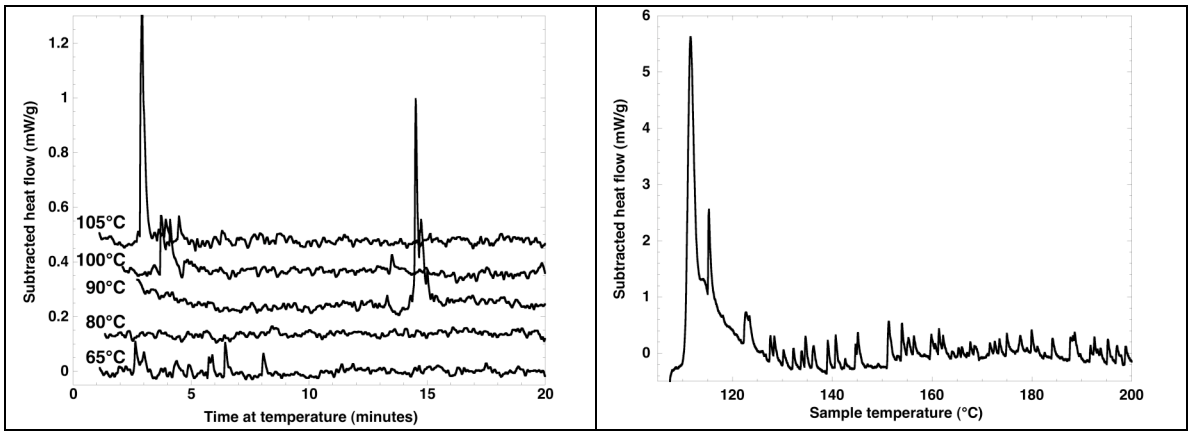

Fig. 14. (a) Isothermal holds at temperatures between 65 °C and 105 °C. The Pu – 2.0 at.% Ga sample was cooled to form α′, heated at 20 °C/min to 65 °C and held for 45 minutes. Following the initial isothermal hold, the temperature was increased in 5 °C increments, with a 45 minute hold at each temperature. Although there is significant noise in the data, some sharp spikes corresponding to the cooperative α′ → δ reversion are evident, particularly at 65 °C, 90 °C, and 105 °C. It is interesting to note that the largest spike at 90 °C occurs after an incubation time of 15 minutes at this temperature. (b) Following the stepped isothermal holds shown in Fig. 14a, the sample was heated at 20 °C/min to complete the α′ → δ reversion. This isochronal scan shows multiple cooperative bursts that extend to temperatures significantly higher than observed when the sample is not held isothermally during the reversion.

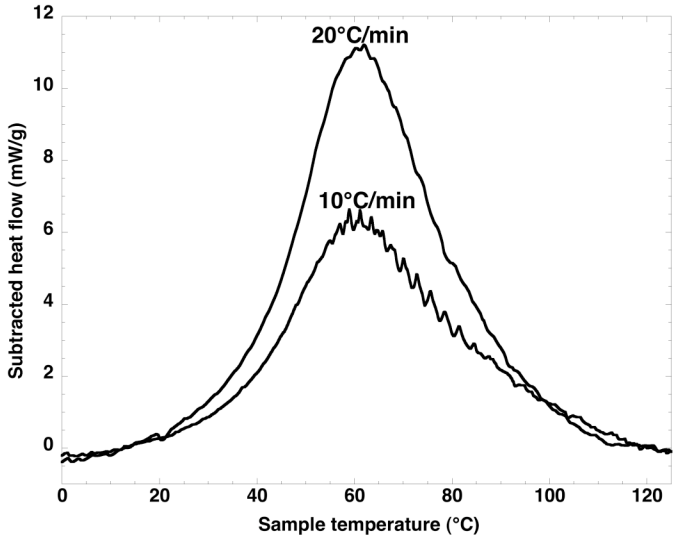

Fig. 15. Isochronal heating scans at 10 °C/min and 20 °C/min showing the range of temperatures over which the α′ → δ reversion occurs (25 °C to 127 °C).

While phase transformations in Pu–Ga alloys are typically observed as a function of temperature using techniques such as differential scanning calorimetry, dilatometry, or resistivity, the isothermal experiments described above demonstrate that there is much to learn about the transformations by studying them as a function of time at fixed temperatures. Additional isothermal studies of the δ → α′ transformation would undoubtedly improve the understanding of the double-C curve in the T-T-T diagram. Furthermore, isothermal studies of the α′ → δ reversion may provide activation energies

and other thermodynamic and kinetic data. Such studies may also help elucidate the remaining questions surrounding phase stability in Pu–Ga alloys.

4.8 Pu–Ga phase diagram and the low-temperature martensite

The connections between the details of the phase diagram in Pu–Ga alloys and the observed features of the martensitic transformations during thermal cycling following conditioning at ambient temperatures are of special interest. To put these transformations into the context of the phase diagram, Massalski and Schwartz [34] considered the likely position of the T_0 trend in the phase diagram for the $\delta \rightarrow \alpha'$ transformation and its possible connection to the data on the onset of the martensitic transformation on cooling (the M_s trend[1]) and its reversal on heating (the R_s trend) at low temperatures. The M_s must be below T_0 and R_s must be above T_0. These trends can be deduced from experimental data obtained by different techniques (e.g., DSC, dilatometry, optical microscopy, resistivity, etc.). However, the actual values of M_s and R_s are a matter of some judgment because they are also affected by the details of each experiment (the cooling rate, sample holding time, composition, homogeneity, grain size, deformation, etc.). It has been shown, for example, that halving the grain size (at small grain sizes) could lower the M_s by some 40–50 °C [61]. The data available on reported M_s and R_s temperatures are plotted in Fig. 3. A comparison between the calculated T_0 trends and the trends of M_s and R_s temperatures was attempted by Massalski and Schwartz and is shown in Fig. 3. As expected, T_0 falls within the mid-space, between R_s and M_s (although the most likely trend maybe somewhat closer to R_s in lower Ga alloys and close to M_s at higher Ga values), as indicated by the "proposed" line.

Using such data, some connections between the phase diagrams, the T_0, and the M_s and R_s transformation temperatures associated with the martensitic transformations can be established. Applied to the particular alloy with a composition of approximately 2 at. % Ga, Massalski and Schwartz [34] argued that, because the Ga composition line for this alloy intersects the calculated T_0 trend at –20 °C, there is about 100 degrees undercooling to drive the martensitic $\delta \rightarrow \alpha'$ transformation at the onset of the upper-C transformations observed in the range of –120 °C. The lower-C curve, initiating below about –145 °C, corresponds in this context to about –125 °C undercooling below T_0, and hence it involves a somewhat larger driving force. Perhaps, because of this, the incubation time prior to the martensitic bursts at the lower-C temperature is somewhat shorter than at the upper C. Both these driving energy values could be estimated, in principle, from phase-field modeling calculations, which utilize free-energy trends and values.

Also of interest is the need to have available sufficient driving force during the "conditioning" time at 25 °C to initiate the formation of embryos of the α phase, prior to the actual occurrence of the martensitic α' bursts later during the cooling cycle. Because the individual martensitic units appear to form in a heterogeneous manner in the matrix, they must be associated with some pre-existing nucleation sites, which become activated on cooling due to the increasing free-energy driving force. Blobaum et al. [36], postulate the formation of initially composition-invariant α embryos during the conditioning at 25

[1] We refer to the onset of the martensitic transformation temperature as M_s. Some authors use M_B to emphasize the burst mode of this transformation.

°C for a few hours. Because the conditioning temperature is some 75 °C below the eutectoid, there is, in principle, adequate driving force for the very early stages of the eutectoid decomposition (which is also assisted by the thermal activations and self-irradiation). If these embryos are initially of the same composition as the δ matrix (i.e., 2 at.% Ga), the undercooling below the corresponding T_0 temperature in the cryogenic region, combined with the thermal activation and self-irradiation effects, must be sufficient to start the transformation. So, the actual value of the T_0 temperature (i.e., the point at which the T_0 trend intersects the temperature axis at 0 at.% Ga) is quite important. Clearly, the fine details of the phase diagram and associated thermodynamics, the phase transformations that occur in the metastable range of the δ phase, the opportunities for some enhanced local diffusion during conditioning, and the subsequent thermal activation in the cryogenic range are all quite critically interrelated.

5. Pressure-induced phase transformations

As discussed above, the δ phase, retained to room temperature, is metastable with respect to the eutectoid decomposition to α + Pu_3Ga at ambient temperature and also metastable with respect to the isothermal martensitic phase transformation at low temperatures. In addition, the δ → α′ phase transformation in Pu-based alloys can also be induced by the application of relatively little pressure, on the order of a few kbar (tenths of GPa). We will begin our discussion of pressure-induced phase transformations by summarizing our literature-based knowledge before describing two sets of new experiments on the pressure-induced δ → α′ phase transformation.

Zukas et al. [59], Hecker [78], and Hecker et al. [41] reported results of the pressure-induced transformation in a well-homogenized Pu – 2 at.% Al alloy. In their study, the authors induce the transformation using quasi-hydrostatic pressure in a Bridgman-type pressure dilatometer. X-ray diffraction and density measurements are used to determine the phases present and the volume fraction of each phase, respectively. Beginning at 0.31 GPa, the δ phase begins to transform to the complex monoclinic β′ phase. Upon release of the pressure, the dilatometry curves reveal an elastic release as well as partial reversion of the β′ phase back to the δ phase. Hydrostatic compression to 1.0 GPa and release to ambient pressure results in a two-phase mixture of 10% β′ and 90% α′. Optical microscopy of the two-phase mixture recorded after intermediate compressions reveals a lath-like β′ phase and a lenticular α′ martensite, which appears to nucleate within the β′ phase. Upon further compression, the α′ martensite consumes the β′ phase while maintaining a lenticular morphology.

Hecker et al. [41] show that the phase transformations under pressure are a strong function of the Ga content; the pressure at which the transformation occurs increases from less than 0.1 GPa for a 1.0 at.% Ga alloy to approximately 0.8 GPa for the 3.5 at.% Ga alloy. They conclude that the transformation occurs directly from δ → α′. The results of the reversion studies after the pressure-induced transformation are similar to those of the isothermal martensite. Low-Ga alloys (<~1.5 at.% Ga), transformed under pressure, revert in a manner similar to the low-temperature δ → α′ transformations. The reversion occurs in an indirect transformation sequence through α′ → β′ → γ′ → δ. On the other hand, high-Ga content (>~1.7 at.% Ga) alloys transformed under pressure are similar to

high-Ga alloys transformed at low temperatures. These alloys undergo a direct reversion from α′ to δ.

Why do Pu–Al alloys transform from δ through β′ whereas Pu–Ga alloys transform directly to α′? Or do they? Recently, Faure et al. [60] performed detailed diamond anvil cell (DAC) experiments on a Pu – 2 at.% Ga alloy using x-ray diffraction to monitor the phases and volumes of the crystal structure as a function of pressure. These experiments conclusively show a $\delta \rightarrow \gamma' \rightarrow \alpha'$ transformation sequence [60]. The intermediate phase, face-centered-orthorhombic γ′, forms concurrently with the monoclinic α′ phase at approximately 0.4 GPa. Their results indicate that the γ′ phase transforms to α′ at about 1.2 GPa. The same transformation sequence is also observed in Pu – 8 at.% Am and Pu – 15 at.% Am alloys. In addition, these authors performed time-dependent experiments by pressurizing a specimen to 1.76 GPa and measuring the unit cell volume as a function of time. The volume is observed to decrease over a period of approximately 300 days before reaching a saturation value. This saturation value is close to that obtained by a slow addition of pressure of 0.1 GPa per day. Both of these atomic volumes are greater than that of unalloyed Pu for the same pressure level.

Hecker et al. [41] described a series of experiments in which α′ was formed either by a low-temperature treatment to induce the isothermal martensitic phase transformation or a pressure-induced transformation. The lattice parameters of the α′ unit cell were measured with x-ray diffraction at ambient temperature and then as a function of time at an annealing treatment slightly above room temperature. In both cases, they observed a decrease in the α′ unit cell volume over that period and suggested that Ga may be migrating to one of eight unique lattice sites within this monoclinic unit cell. Sadigh and Wolfer performed density-functional theory (DFT) calculations in which the molar volume of a Ga atom was determined for each of the eight unique sites in the 16-atom monoclinic α′ unit cell [72]. The results indicate that indeed the lowest energy configuration occurs when the Ga atom substitutes for a Pu atom in the largest volume site in a Voronoi cell construction, site 8, as determined from x-ray diffraction experiments [79,80]. Does the time dependence of the α′ volume change suggest Ga hopping to site 8? Experimental determination of the Ga occupation on site 8 – in samples with higher Ga content – using techniques such as Extended X-Ray Absorption Fine Structure (EXAFS) would shed some light on these calculations.

Very recently, Harbur [43] expanded the discussion on the pressure-induced phase transformation investigation described in Hecker et al. [41]. Based on x-ray diffraction, density, and compressibility experiments, Harbur [43] concludes that both α′ and an amorphous phase are present in samples that were pressurized and recovered. There was, however, no direct evidence of an amorphous phase via XRD; the presence of the non-crystalline material was argued on the basis of density analysis. In a Pu – 0.68 at.% Ga alloy that was well homogenized and cooled to room temperature, the density was observed to be intermediate between unalloyed α and δ. X-ray diffraction revealed diffraction peaks only from the α′ phase leading to the conclusion of the presence of an amorphous phase. Results from alloys containing 1.0, 1.7, and 2.5 at.% Ga that were compressed to 1 GPa revealed similar results. The densities were intermediate between α and δ and x-ray diffraction exhibited only α′ peaks. Harbur concludes the percentages of the phases after compression and recovery to be as shown in Table 1.

Table 1
Percentages of α′, δ, and amorphous phases after compression to 1 GPa and release to ambient pressure for three different alloys [43].

Ga content (at.%)	% α′	% δ	% amorphous
1.0	87	0	13
1.7	66	0	34
2.5	68	12	20

5.1 Diamond anvil cell

Over the past several years, we have performed x-ray diffraction experiments to evaluate the pressure-induced phase transformations of δ-stabilized Pu (Pu – 3.3 at.% Ga) at room temperature using modern diamond anvil cell techniques. The experiments are performed using Lawrence Livermore National Laboratory-designed membrane-driven DACs with 500 μm flat diamond anvils. Rhenium gaskets are pre-indented to thicknesses of ~50 μm and drilled with sample chamber holes of ~200 μm. The δ-stabilized Pu samples for study are cut from a foil specimen, electropolished to remove oxide, contaminants, or fabrication-induced second phases at the surface, and placed in EM Science-USP Chemicals EM-MX1560-1 mineral oil to inhibit degradation. Working in an argon-purged glove bag, a ~1 μg piece is carefully cut from the cleaned foil and loaded into the DAC gasket hole. A few micron-sized particles of ruby are also placed in the gasket hole for *in-situ* pressure determination during the x-ray diffraction experiments. Any remaining space in the sample hole is filled with mineral oil, which serves as the hydrostatic pressure media in all of the experiments.

The x-ray diffraction measurements are performed using modern third generation synchrotron techniques at the HPCAT beamline (16ID-B) at the Advanced Photon Source. The diffraction technique is monochromatic angle-dispersive x-ray diffraction using x-ray beam diameters of ~20 μm and a wavelength of 0.39 Å. The diffracted x-ray signal is detected using an image plate (MAR-345) with exposure times of ~30 seconds. The Debye-Scherrer x-ray diffraction ring images are collapsed to 1-dimensional intensity *vs.* 2Θ patterns using the Fit2d software package. The pressure is determined *in situ* using the ruby fluorescence technique [81]. Pressure determinations based on ruby fluorescence are accurate to better than 0.1 GPa. The volume determinations, derived from the measurements of the crystal structures and lattice constants, have accuracies of better than 0.3%.

These results show the δ → γ′ → α′ pressure-induced transformation path, which is entirely consistent with the recently reported studies by Faure et al. [60]. With increasing pressure, a multiphase mixture of δ′ + γ′ + α′ is formed at 0.4 GPa and persists up to 1.4 GPa. Beyond 1.4 GPa, δ′ disappears, leaving a γ′ + α′ mixture, which persists for only a 0.2 GPa pressure range, leaving only α′ beyond 1.6 GPa. Representative diffraction spectra showing this progression are provided in Fig. 16 and the respective existence and volume of the phases is shown as a function of pressure in Fig. 17. At very low pressure we observe line broadening from the initial δ phase to a phase we denote as δ′ due to the body-centered-tetragonal structure that is similar to the high-temperature δ′ phase

observed in pure Pu (see Fig. 18). The indicator of this δ′ phase is a broadening of the diffraction peaks, which we interpret as unresolved line splittings.

An issue we have not directly addressed is the kinetics of the transformation, but we do not believe kinetics impacts these observations. The data presented are a composite of five separate experimental runs (same material source, but different samples), and the time between each XRD measurement (detector exposure, readout and pressure increase) is several minutes. If kinetics influences the transformation, the data would not have been consistent between different experimental runs.

We note that even at the start of our experiments at ambient pressure, we observed weak diffraction peaks characteristic of the α′ phase. We interpret this to mean that typical preparation and handling procedures are sufficient to induce a small amount of metastable transformation to the α′ phase.

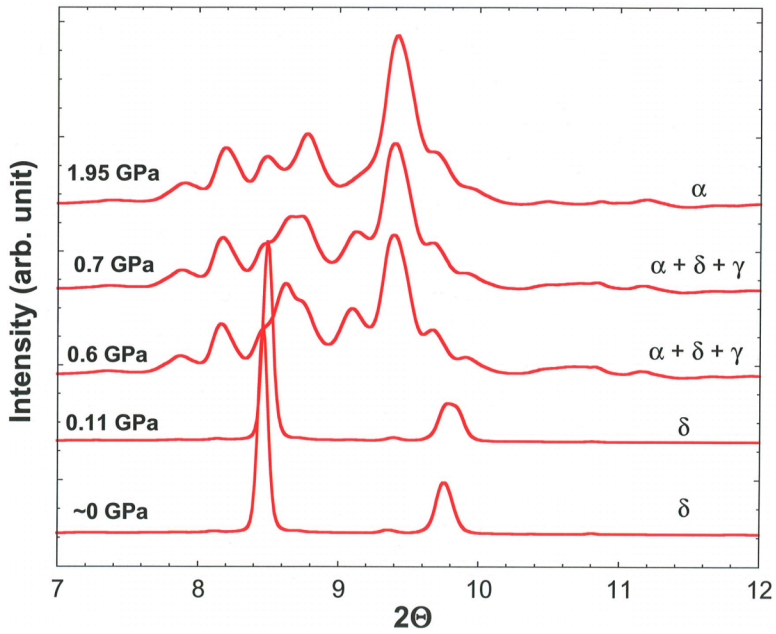

Fig. 16. Intensity versus 2Θ plots showing pressure-induced transformations of δ-Pu (Pu – 3.3 at.% Ga) up to 1.95 GPa. The initial δ-phase sample transforms to a mixture of α′ and γ′, finally transforming to 100% α′ at 1.95 GPa, the highest pressure of these studies. Very weak α′ peaks can be seen at the lowest pressure. These weak peaks are likely a result of pressure-induced transformations caused during the sample preparation (mechanical deformation due to cutting).

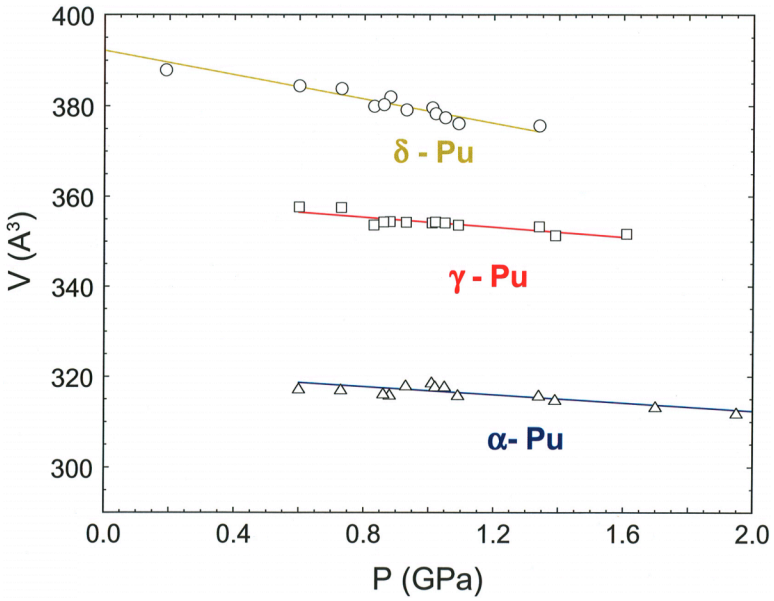

Fig. 17. A plot of volume versus pressure, showing the pressure-induced progression through the δ (δ′), γ′ and α′ phases. The δ (δ′), γ′ and α′ phases are shown as open circles squares, and triangle, respectively. A line is drawn through each phase as a guide. There is a broad coexistence regime between 0.6 and 1.35 GPa.

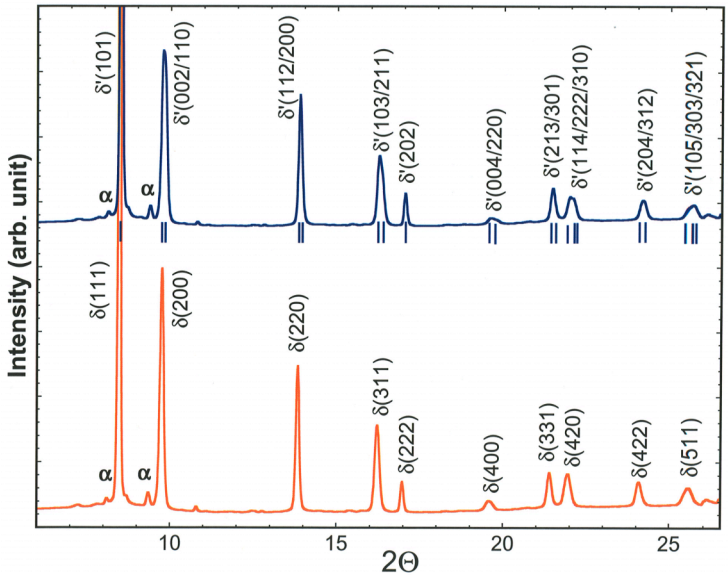

Fig. 18. Comparison of representative plots of the δ and δ′ phases at very low pressure (~0 GPa). The lower trace shows a δ-Pu XRD pattern with indexing of diffraction peaks noted. The upper trace shows a δ′-Pu XRD pattern with peak splitting, manifested as line broadening, which is indexed as a body-centered-tetragonal crystal structure.

5.2 Large-volume moissanite anvil cell

In this work, a large-volume moissanite anvil cell was constructed to permit the pressurization and recovery of specimens of a size suitable for subsequent TEM and electron diffraction studies. The cell, shown in Fig. 19, has an overall diameter of 101.6 mm, a moissanite (SiC) anvil diameter of 9.00 mm, a culet size of 3 mm, and a spring

steel gasket 0.5 mm thick with a hole diameter of 2.5 mm. A 2.3 mm diameter by 100 μm thick sample of δ-phase Pu – 2 at.% Ga is compressed in Dow Corning silicone oil at a rate of approximately 0.05 GPa/minute to ~1 GPa to induce the phase transformation to α′.

Optical microscopy of the recovered specimen reveals a very fine microstructure of what appears to be a single phase, although the resolution of this technique is insufficient to differentiate between single and multiple phases if the grain size is below approximately 1 μm. X-ray diffraction, using a laboratory Cu K_α source with wavelength of 1.542Å, shows reflections from the monoclinic α′ phase, strong peaks from the aluminum specimen holder, and weak peaks from the face-centered-cubic δ phase as shown in Fig. 20. The recovered specimen was then prepared for TEM and electron diffraction studies as described in Moore et al. [82].

TEM reveals small regions of δ phase with a very high dislocation density between the 10 – 100 nm α′ grains as shown in Fig. 21. Electron diffraction, shown in the insert in Fig. 21, clearly reveals the presence of the dominant α′ phase and the lower volume fraction δ phase. This microstructure, resulting from a partial pressure-induced phase transformation, is in contrast to the α′ particles that form as a result of the low-temperature isothermal martensitic phase transformation in which the α′ particles are lath-shaped and significantly larger, as shown in the optical micrograph in Fig. 4 of a sample cooled to –155 °C and held for 4 hours and subsequently observed at room temperature.

The microstructure of the α′ particles significantly differs from one would generally expect in martensitic phase transformations in which planar interfaces, some evidence of an orientation relationship, elongated grains, and significant faulting within the martensite are typically observed. At this point, it is unclear how a martensitic transformation could result in such an uncharacteristic microstructure. It is possible that when these alloys are cooled, the driving force is small and only causes the most energetically favorable embryos to burst into α′ particles. These are limited in number and can grow to rather large sizes due to limited interaction of the strain fields. Under pressure, however, the driving force is greater. Thus, a larger number of embryos nucleate into α′, but due to the high density of α′ particles, the grain size is quickly limited by the impingement on other growing α′ grains. In these preliminary *post mortem* results, there is also no evidence based on x-ray diffraction or TEM and electron diffraction of either an amorphous phase, as suggested by Harbur [43], or the presence of a γ′ phase. One would have expected to detect an amorphous phase based on the similarity of this experiment to that of Harbur [43]. The results of the DAC experiments, first reported by Faure et al. [60] and also reported here, indicate that the 1 GPa pressure was sufficient to form the γ′ phase. It is unclear at this time whether the γ′ phase reverts back to δ upon the release of pressure, or partially transforms to the α′ phase upon the release.

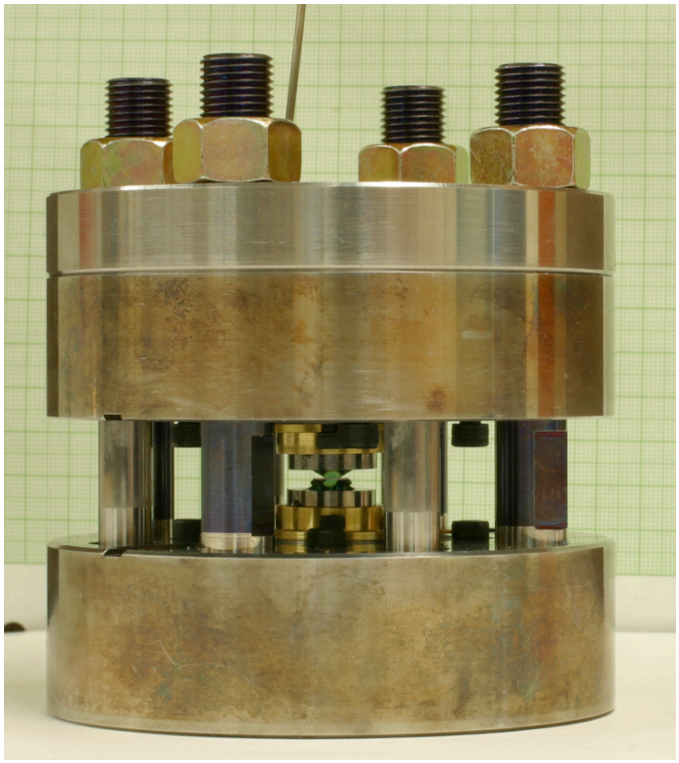

Fig. 19. Photograph of large volume moissanite anvil cell used for compressing TEM-sized samples.

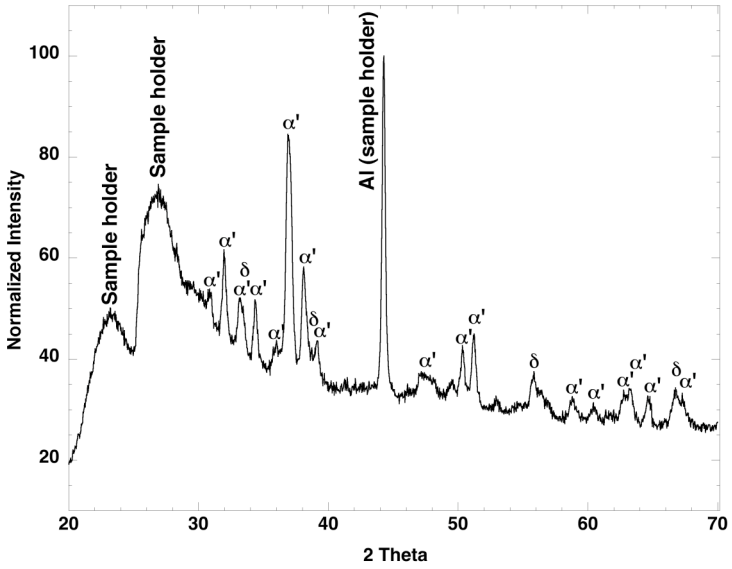

Fig. 20. X-ray diffraction pattern taken from a Pu – 2.0 at.% Ga sample that was compressed to 1 GPa and characterized at ambient pressure. Strong α′ peaks and weak δ peaks are evident.

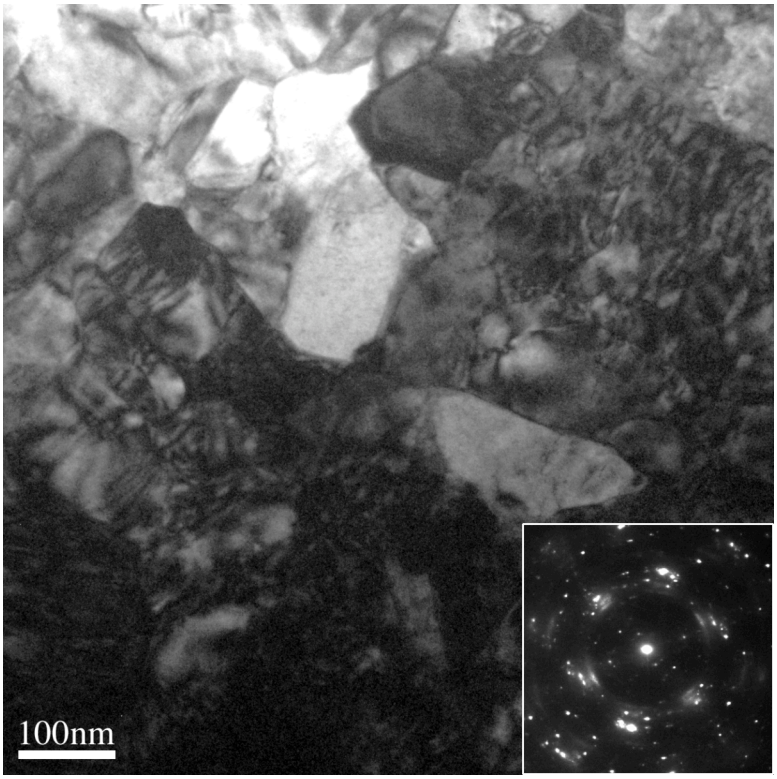

Fig. 21. Bright-field TEM image of a Pu – 2.0 at.% Ga sample that was compressed to 1 GPa and characterized at ambient pressure. The insert shows an electron diffraction pattern from a neighboring area that reveals Bragg peaks from both the α' and δ phases.

5.3 Coupling of theory, modeling, and experiments

5.3.1 Recent advances

Recent experiments probing the electronic structure [83-90], advances in the theoretical understanding of correlated electron systems [91,92], and significantly enhanced computational power have had an increasing role in contributing to our understanding of the electronic structure and ground state energies of the actinides, particularly Pu. Electron energy-loss spectroscopy (EELS) within the TEM has been demonstrated to be substantially equivalent to x-ray absorption spectroscopy experiments [93] and has led to significant insight into the delocalized-to-localized electron transition [87-90]. Electron energy loss spectroscopy experiments indicate that the actinides from Pu through Cm are best modeled with the "intermediate coupling" approximation, due to the balance between exchange and spin-orbit interaction rather than the Russell-Saunders *(LS)* or the *jj*-coupling schemes [88,89]. For Pu, intermediate coupling is very near the *jj* limit due to the strong spin-orbit interaction of the 5*f* states. These experiments have also suggested that the number of 5*f* electrons in Pu is much closer to $n_f = 5$ than $n_f = 6$, as already indicated by the recent dynamical mean-field theory calculations (mean-field theory calculations of lattice dynamics) [89,94]. Furthermore, EELS, coupled with atomic spectral calculations and density-functional theory calculations, provide strong

indications that spin-orbit coupling of the 5*f* states contributes considerably to the ground state energies of the Pu allotropic phases [88,89]. This indirectly suggests that spin polarization is of minor importance for Pu, but is highly important for Cm. These advances in experimental techniques and theoretical calculations enabled Moore et al. [89] to show how magnetism is vital to the phase stability of the crystallographic phases of Cm. Advances in dynamical mean-field theory over the past decade [95] have allowed the calculations of the frequencies (ω) of the modes of vibrations (phonons) in relation to their wave vectors (k), known as the phonon dispersion relationship. For the unalloyed δ phase, this calculation has predicted the most likely phonon dispersion curve, which is very similar to the subsequently published experimental determination on a Pu – 2 at.% Ga alloy of the same relationship, using high-resolution inelastic x-ray scattering [96,97]. Coupling of experiments and theory appears to be the best approach to further extend our understanding of the complex electronic structure and the physical properties of the actinides.

As already mentioned above, there have been accumulating theoretical indications [7,98,99] and experimental evidence [100-103] that δ-phase Pu alloys at ambient conditions are metastable and are susceptible to a reduction in symmetry from the high-symmetry fcc structure to a lower-symmetry structure. Which lower-symmetry structure the δ-Pu phase tends to develop has not been conclusively established with the experimental techniques that have been used, such as TEM, neutron diffraction, or x-ray diffraction [53,101]. Under pressure, as described above, the fcc δ-Pu crystal structure distorts to the body-centered tetragonal crystal structure and the changes are of sufficient magnitude to allow indexing of the x-ray diffraction patterns with some confidence. Without pressure, the distortions of the crystal structure measured at ambient temperature and pressure are apparently too small in magnitude to be indexed with significant reliability. However, since it is quite evident that the fcc δ phase is readily susceptible to a lowering of the crystal structure symmetry under pressure, it may be also on the verge of a reduction of symmetry at ambient conditions.

5.3.2 Density-functional theory calculations

Building on the successes of the density-functional theory calculations for transition [104] and actinide [105] metals, Moore et al. [106,107] applied density-functional theory using the full-potential linear-muffin-tin orbital (FPLMTO) [108] approach to calculate the bond strengths of the 12 nearest neighbors in the fcc δ-Pu structure. The "full potential" refers to the incorporation of non-spherical contributions to the electron charge density. This is accomplished by expanding the non-spherical contribution in cubic harmonics inside non-overlapping muffin-tin spheres and in a Fourier series in the interstitial region. For the electron exchange and correlation energy functional, the generalized gradient approximation (GGA) was adopted [109]. The nearest-neighbor bond strengths were obtained from total energy calculations based on a 27-atom super cell that uniquely defines all 12 nearest neighbors (NN). By introducing small (2%) displacements along each of the 12 NN bonds, the force associated with the respective bond can be evaluated from the corresponding energy change divided by the magnitude of the displacement. The authors interpreted these calculated forces as the respective "bond strengths." Although it has been shown that spin-orbit coupling is an important

factor in the 5*f* states of Pu, the authors proposed that the spin-orbit interaction can be replaced by ferromagnetic spin polarization to simplify the calculations. The authors justify this simplification because it has been shown that the spin-orbit splitting that occurs in the 5*f* states is very much like the ferromagnetic ordering and also that this assumption nevertheless allows one to derive experimentally observed values of the equilibrium volume, bulk modulus, and elastic constants.

The 12 nearest neighbor bond strengths as calculated by density-functional theory are listed in Table 2, where the nearest neighbor direction (*x,y,z*), Miller indices (*h,k,l*), change in energy (ΔE) due to a 2% shift of the (0,0,0) atom, and the change in energy (ΔE) normalized by the displacement length (u) are given as (ΔE/u) [106,107]. The nearest neighbor bond strengths are also illustrated in Fig. 22, which gives a visual representation of the results. Readily noticeable is that ΔE/u varies significantly from ~3.3 to ~5.3 mRy/Å, showing the large degree of variation in bond strength between the 12 nearest neighbors. Although it is interesting to note that the calculated bonds in the {001} planes are almost the same directly across each central atom, the bonds in the {011} planes are not uniform and reveal a more complicated relationship. No interpretation of this result is available at this time. It is possible that this difference in bond behavior can be related to the observed "phonon softening" in certain lattice directions. Speculating further, it may be possible that this softening facilitates in some way the δ → α′ phase transformation in dilute Pu-Ga δ-phase alloys.

Table 2
The nearest neighbor direction in *x*, *y*, *z* coordinates, Miller indices (*h k l*), and bond strength *F* (mRy/Å) for pure Pu and a gallium atom in a Pu – 3.7 at.% Ga alloy.

Nearest Neighbor Direction	**Miller Indices**	**Pure Pu**	**Pu-3.7 at.% Ga**
(*x*, *y*, *z*)	(*h k l*)	*F* (mRy/Å)	*F* (mRy/Å)
(0.5, 0.5, 0)	110	4.7	6.3
(-0.5, -0.5, 0)	$\bar{1}\bar{1}0$	4.5	6.1
(0.5, -0.5, 0)	$1\bar{1}0$	3.7	6.3
(-0.5, 0.5, 0)	$\bar{1}10$	3.5	6.4
(0.5, 0, 0.5)	101	4.1	7.0
(-0.5, 0, -0.5)	$\bar{1}0\bar{1}$	3.3	5.6
(-0.5, 0, 0.5)	$\bar{1}01$	4.7	4.4
(0.5, 0, -0.5)	$10\bar{1}$	3.9	5.5
(0, -0.5, 0.5)	$0\bar{1}1$	3.9	7.3
(0, 0.5, -0.5)	$01\bar{1}$	3.3	5.9
(0, 0.5, 0.5)	011	5.3	6.0
(0, -0.5, -0.5)	$0\bar{1}\bar{1}$	3.7	6.0

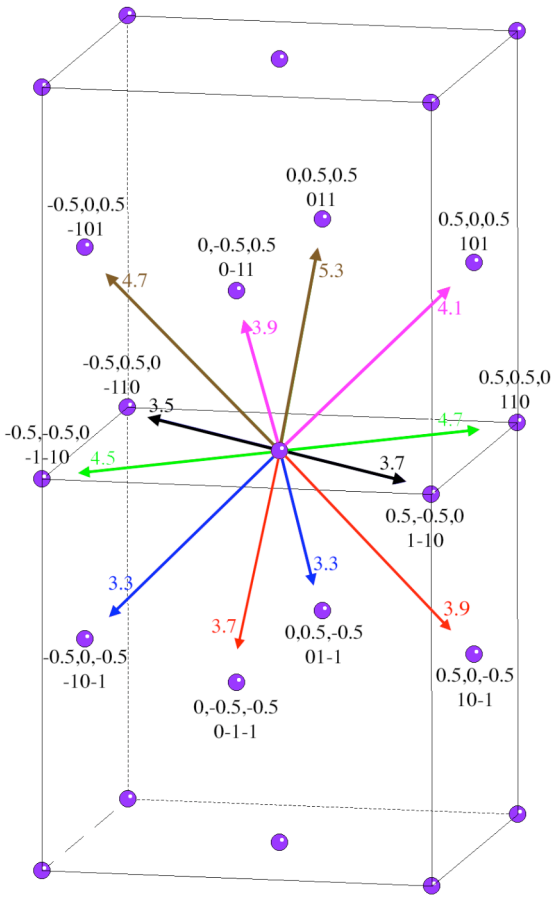

Fig. 22. Two stacked fcc unit cells with the central atom showing the 12 nearest neighbors. In the case of plutonium, the 12 bonds with the nearest neighbors vary widely in strength and can be separated into six pairs: blue (3.3), black (3.5-3.7), red (3.7-3.9), pink (3.9-4.1), green (4.5-4.7), and brown (4.7-5.3). When the fcc lattice is combined with the motif of these bond strengths the resultant space group is monoclinic *Cm*. The bond strengths as calculated with density-functional theory of the twelve nearest neighbors can be separated into six pairs of two where the bond strengths are close in value: blue (3.3), black (3.5-3.7), red (3.7-3.9), pink (3.9-4.1), green (4.5-4.7), and brown (4.7-5.3). In the (001) plane, the [110] bond is roughly equal to the $[\,\bar{1}\bar{1}0\,]$ bond (green), and the $[\,\bar{1}10\,]$ bond is roughly equal to the $[\,1\bar{1}0\,]$ bond (black). In the {011} planes, however, we see that $[\,01\bar{1}\,]\sim[\,\bar{1}0\bar{1}\,]$ (blue), $[\,0\bar{1}\bar{1}\,]\sim[\,10\bar{1}\,]$ (red), $[\,0\bar{1}1\,]\sim[\,101]$ (pink), and $[\,011]\sim[\,\bar{1}01]$ (brown).

The results of the calculations indicate that when a motif of the calculated bond strengths is added to the fcc lattice, as is done in crystallographic constructions, the resultant crystal structure is reduced from fcc to *c*-centered monoclinic with the space group *Cm*. This low-symmetry space group lacks rotational symmetry and includes only one mirror plane along the (110) plane. The Bravais lattice for the *c*-centered monoclinic structure is shown in Fig. 23.

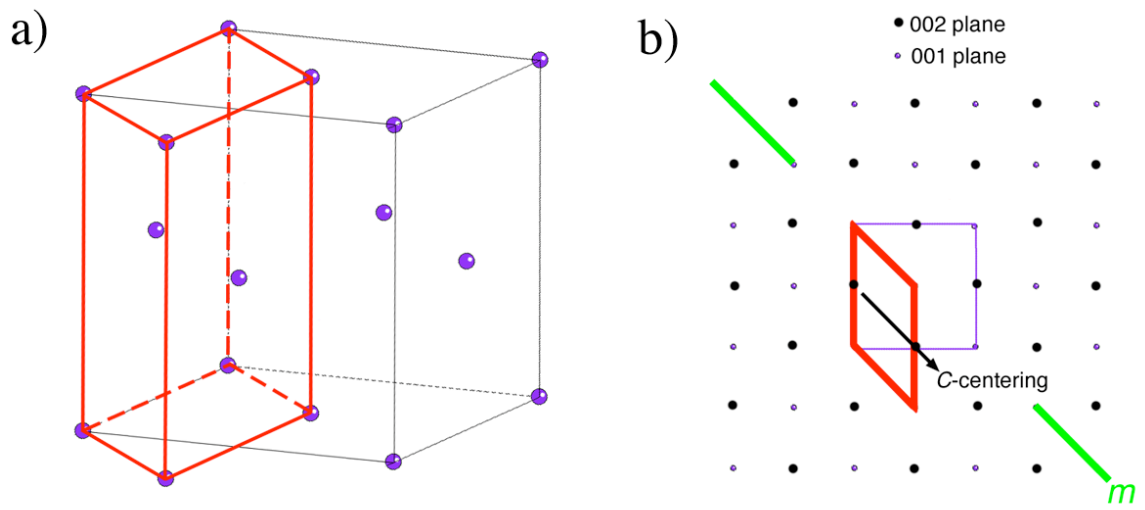

Fig. 23. The Bravais lattice of the *c*-centered monoclinic unit cell. (a) The three-dimensional rendering of the *c*-centered unit cell and (b) a two-dimensional rendering viewed along the [001] direction where the fcc lattice is shown by the purple box. The *c*-centered unit cell is shown by the heavy red box with the green line marking the [110] mirror plane.

As a check of their computational approach, Moore et al. performed similar calculations for Al, the most isotropic fcc metal [106,107], as they did for Pu and a Pu – 3.7 at.% Ga alloy. The results show that the 12 bonds in Al are all equal in strength and hence retain the $m\bar{3}m$ bond-strength symmetry. Thus, the fcc structure of Al should be highly symmetric.

To evaluate the effect of gallium on the symmetry of fcc δ-phase, similar calculations to those described above were performed with a Ga atom in the central position of the 27-atom super-cell being subjected to the same magnitude of displacement. In this case, the authors find that the 12 bond strengths calculated with a 2% displacement differ less drastically than in the case of pure Pu (see Table 2). The majority of bond strengths are near F = 6 mRy/Å with the exception of [010] (F = 7.0), $[0\bar{1}1]$ (F = 7.3), and $[10\bar{1}]$ (F = 4.4). Why these bond forces in the particular directions are so high and low in value is not clear; however, the other 9 bonds are near F = 6 and are thus rather uniform. The uniformity in force implies that the bond strengths surrounding the Ga atom are on the whole higher in symmetry, thus resembling a higher-symmetry fcc structure. The authors conclude that these calculations illustrate why the presence of Ga tends to stabilize the higher-symmetry fcc δ-phase over a wider range of temperatures, than in pure Pu, by making the bond strengths in the local regions about each Ga atom less anisotropic. An important question to ask is whether any substitutional atom would have the same effect as Ga. It will be of interest to see if a uranium atom, which is known to be an α-phase stabilizer, would have the same effect as Ga or would tend to enhance even larger anisotropic bond strengths than those in unalloyed Pu.

The extended X-ray absorption fine-structure spectroscopy (EXAFS) results of Cox et al. [102] support the conclusions of the calculations for the both pure Pu and the Pu – 3.7 at.% Ga alloy. In their experiments on Ga-stabilized δ-Pu, it was observed that the local structure of plutonium around the Ga atoms was well defined and similar to a typical fcc metal. However, the local structure of plutonium around Pu atoms was less

uniform. The density-functional theory calculations show exactly that: the bonds in pure Pu are highly anisotropic and thus deviate substantially from a typical fcc structure, whereas the bonds about a Ga atom are more isotropic and thus deviate less from the fcc structure. Extended X-ray absorption fine-structure spectroscopy has also shown that there is a local contraction of the lattice around Ga atoms in Pu–Ga alloys [110]. This is also observed in the calculation as shown in Table 2 where the bond forces between pure Pu atoms are around $F = 4$, whereas the bond forces between Pu and Ga atoms are around $F = 6$. These higher bond forces imply the strength of the bonds is greater and accordingly would cause a contraction of the lattice in certain directions as observed by EXAFS. Finally, recent high-temperature thermal conductivity measurements by Alexander and Wood [103] also support some form of distortion from fcc symmetry in δ-Pu.

6. Concluding remarks and future directions

Arguably, the most interesting challenge in understanding the $\delta \rightarrow \alpha'$ isothermal martensitic phase transformation is the cause of the double-C curve kinetics. Although significant efforts have been expended in both continuous cooling and isothermal holding experiments leading to increased understanding about the crystallography and morphology of this transformation, focused experiments are essential to characterize the change in crystal structure as a function of time at low temperatures, including the exothermic reaction that occurs at temperatures above the knees in the T-T-T plots. Critical experiments have been attempted *in situ* within the TEM or at synchrotron sources to follow the crystallographic changes as a function of continuous cooling or as a function of time at sub-ambient temperatures. However, both of these experiments used a thin foil – less than 50nm thick for the TEM and approximately14 μm thick for the synchrotron – and in each case, the probe did not resolve or detect the crystallography of the phase transformation. It is possible that the thinness of the specimen and the associated surface stresses retard the transformation. Looking forward, *in situ* neutron diffraction on ^{242}Pu or x-ray diffraction of bulk specimens at a synchrotron or high brightness sources may provide the critical information regarding the transformation path.

The powerful effects of conditioning on the amount of transformation product are quite evident. However, the precise origin of this time-dependent effect remains unknown. Annealing in the TEM followed by imaging characterization of the microstructure as a function of time may provide direct observable evidence of embryo formation in the early stages. Indirect probes, such as resistivity, might be used to detect a progressive change that occurs on the order of a few hours. The annealing temperature and times required to destroy the effects of conditioning have yet to be examined.

Answering these questions about the time scales involved in conditioning is just the beginning of elucidating the time-dependent changes in Pu-based alloys. Baskes et al. [111] evaluated the nearest-neighbor ordering tendencies in a Pu – 5 at.% Ga alloy using molecular dynamics and kinetic Monte Carlo methods. These results suggest that short-range order develops in very short times (~10,000,000 time steps). Compare this to the effects of conditioning that saturate in approximately six hours, and to the changes in the lattice parameter that saturate in three months, and the size of the helium bubbles that

appears to saturate in approximately ten years. Reconciling the atomistic processes that dictate this range of time scales is certainly a formidable task—one that must be addressed to further our understanding of the structures and phase transformations.

Recent diamond anvil cell experiments on Pu – 2 at.% Ga alloys reported here and by Faure et al. [59] provide conclusive evidence regarding the formation of the intermediate face-centered-orthorhombic γ' phase during the hydrostatic compression of the δ phase. This sequential transformation in the Pu – 2 at.% Ga alloys of $\delta \rightarrow \gamma' \rightarrow \alpha'$ differs from that reported by Zukas et al. [59] for Pu – 2 at.% Al, which undergoes the transformation sequence $\delta \rightarrow \beta' \rightarrow \alpha'$. In both the Faure et al. experiments and the experiments described above, small specimens of Pu–Ga were compressed, while larger samples of Pu–Al were used by Zukas et al. It is unclear at this time why the same amount of Al and Ga substitution has such a dramatic effect on the intermediate phase. High-resolution x-ray diffraction experiments on specimens of a Pu – 2 at.% Al alloy compressed in the DAC would determine whether the difference in transformation sequence results from sample size or from fundamental physics.

Both sets of DAC experiments strongly indicate that at 1 GPa there exists a three phase mixture of δ (or δ'), γ', and α'. Upon release of the pressure, it is unclear what happens to the γ' phase. It is likely that the γ' reverts back to δ as indicated in the large-volume moissanite anvil cell recovery experiments, but additional *in situ* experiments should quantify the fractions of the phases present both during hydrostatic compression to 1 GPa and during release to ambient pressure. Future experiments should probe both lower and higher pressures, the effects of time at pressure, and the kinetics of γ' reversion.

The description of the fcc crystal symmetry and the phonon dispersion curves in relation to density-functional theory, atomic spectral calculations, and electron energy-loss spectroscopy in elucidating aspects of the electronic structure have all demonstrated the powerful outcomes resulting from thoughtful coupling of theory and experiments. This same approach will undoubtedly be helpful for enlightening our understanding of the intermediate phases that have been shown to exist in the pressure-induced transformation and the suggestions of an intermediate phase in the low-temperature martensitic phase transformation in Pu – Ga alloys. A first attempt at this was recently reported by Lookman et al. [75] where they describe the symmetries of the $\delta \rightarrow \alpha'$ phase transformation path. That work, which applies the modified embedded atom potential should be supplemented with first-principles calculations and phase-field modeling to further our understanding of these complex and rather unique phase transformations.

In recent years, the Pu science community has gained an increased understanding of the eutectoid transformation, equilibrium phase diagram, metastability of the δ phase, crystallography of the α' phase, burst characteristics of the $\alpha' \rightarrow \delta$ reversion transformation, and the importance of a conditioning treatment. We have become convinced of an intermediate transformation to γ' on the path from $\delta \rightarrow \alpha'$ during the pressure-induced transformation. We have seen the powerful outcomes of the advances and applications of density-functional theory, dynamical mean-field theory, and molecular dynamics [112] enabled by high performance computing. Once again, however, it appears that the more we learn about Pu and its alloys, the more research is required to fully understand the fundamental science underlying this challenging material.

Acknowledgements

This work performed under the auspices of the U.S. Department of Energy by Lawrence Livermore National Laboratory under Contract DE-AC52-07NA27344. Work performed at HPCAT was supported by DOE-BES, DOE-NNSA, NSF, DOD-TACOM, and the W.M. Keck foundation. Use of the Advanced Photon Source was supported by the U.S. Department of Energy, Office of Science, Office of Basic Energy Sciences, under Contract No. W-31-109-ENG-38. The authors acknowledge use of the program FIT2D developed by A. Hammersley of ESRF.

References

[1] Gibbs JW. Elementary principles in statistical mechanics. New Hampshire: Yale University Press; 1902.
[2] Wirth BD, Schwartz AJ, Fluss MJ, Caturla MJ, Wall MA, Wolfer WG. Fundamental Studies of Plutonium Aging. MRS Bulletin 2001;26(9):679-683.
[3] Howell RH, Sterne PA, Hartley J, Cowan TE. High energy beam lifetime analysis. Appl Surf Sci 1999;149:103-5.
[4] Schwartz AJ, Wall MA, Zocco TG, Schaldach C, Wolfer WG. Characterization and modeling of helium bubbles in self-irradiated plutonium alloys. Phil Mag 2005;85(4-7):479-488.
[5] Rohr DR, Staudhammer KP. First observations of microstructural changes in delta Pu by transmission electron microscopy. J Nucl Mater 1987;144:202-4.
[6] Wolfer WG. Radiation effects in plutonium – What is known? Where should we go from here? In: Cooper NG, editor. Los Alamos Science, No. 26, Challenges in Plutonium Science, Los Alamos, Los Alamos National Laboratory; 2000, p. 274-285.
[7] Valone SM, Baskes MI, Martin RL. Atomistic model of helium bubbles in gallium-stabilized plutonium alloys. Phys Rev B 2006;73:214209.
[8] Arsenlis A, Wolfer WG, Schwartz AJ. Change in flow stress and ductility of δ-phase Pu-Ga alloys due to self-irradiation damage. J Nucl Mater 2005;336:31-39.
[9] Kubota A, Wolfer WG, Valone SM, Baskes MI. Collision cascades in pure δ-plutonium. J Computer-Aided Mater Des 2007;14:367-378.
[10] Fluss MJ, Wirth BD, Wall MA, Felter TE, Caturla MJ, Kubota A, Diaz de la Rubia T. J Alloys and Comp 2004;368:62-74.
[11] Wolfer WG, Söderlind P, Landa A. Volume changes in δ-plutonium from helium and other decay products. J Nucl Mater 2006;355:21-9.
[12] Wolfer WG, Oudot B, Baclet N. Reversible expansion of gallium-stabilized δ-plutonium. J Nucl Mater 2006;359:185-191.
[13] Wolfer WG, Kubota A, Söderlind P, Landa AI, Oudot B, Sadigh B, et al. Density changes in Ga-stabilized δ-Pu, and what they mean. J Alloys Comp 2007;444-445:72-9.
[14] Ravet B, Oudot B, Baclet N. Study by XRD of the lattice swelling of PuGa alloys induced by self-irradiation. J Nucl Mater 2007;366:288-296.

[15] Freibert FJ, Dooley DE, Miller DA. Formation and recovery of irradiation and mechanical damage in stabilized δ-plutonium alloys. J Alloys Comp 2007;444-445:320-4.
[16] Chung B, Schwartz AJ, Ebbinghaus BB, Fluss MJ, Haslam JJ, Blobaum KJM, Tobin JG. Spectroscopic signature of aging in δ-Pu(Ga). J Phys Soc Japan 2006;75(5):054710.
[17] Migliori A, Mihut I, Betts JB, Ramos M, Mielke C, Pantea C, Miller D. Temperature and time-dependence of the elastic moduli of Pu and Pu–Ga alloys. J Alloys Comp 2007;444-445:133-7.
[18] Martz JC and Schwartz AJ. Plutonium: Aging Mechanisms and Weapon Pit Lifetime Assessment. JOM 2003;55(9)19-23.
[19] Hecker SS. Plutonium – an Element Never at Equilibrium. Met Mat Trans 2008;39A:1585-1592.
[20] Ellinger FH, Land CC, Struebing VO. The plutonium-gallium system. J Nucl Mater 1964;12(2):226-236.
[21] Schonfeld FW. Plutonium phase diagrams studied at Los Alamos. In: Coffinberry AS, Miner WN, editors. The metal plutonium, Chicago: The University of Chicago Press; 1961, p. 240-264.
[22] Hocheid B, Tanon A. Bedere S, Despres J, Hay S, Hiard F. Studies of the binary systems plutonium–gold, plutonium–gallium, and plutonium–indium. In: Kay AE, and Waldron MB, editors. Plutonium 1965, London; Chapman and Hall 1967, p. 321-340.
[23] Peterson DE, Kassner ME. Bull Alloy Phase Diagr 1988;9(3):271-7.
[24] Bochvar AA, Konobevsky ST, Kutaitsev VI Menshikova TA, Chebotarev NT. Interaction of plutonium and other metals. In: Proceedings of the 2nd United Nations International Conference on the Peaceful Uses of Atomic Energy, United Nations, Vol. 3, Geneva: 1959, p. 376-395.
[25] Chebotarev NT, Smotriskaya ES, Andrianov MA, Kostyuk OE. Some results of a study of the Pu–Al–Ga phase diagram. In: Blank H, Lindner R, editors. Plutonium 1975 and Other Actinides, Amsterdam: North Holland Publishing Co; 1975, p. 37-46.
[26] Timofeeva LF. Some regularities in eutectoid transformations in binary systems of plutonium. Atomic energy 2003;95(2):540-5.
[27] Timofeeva LF. Low temperature equilibrium aging under self-irradiation in binary alloys of plutonium with elements of the IIIB group. In: Mallison L. editor. Proc. Int. Conf. On Ageing Studies and Lifetime Extension of Materials, Dordrecht: Kluwer Academic Publishers; 2000, p. 191-8.
[28] Timofeeva LF. Phase transformations in Pu–Ga and Pu–Al alloys – Effects of pressure and temperature on kinetics of δ-phase decomposition. J Alloys and Compounds 2007;444-445:124-128.
[29] Adler PH. Thermodynamic equilibrium in the low-solute regions of Pu-group IIIA metal binary systems. Met Trans 1991;22A:2237-2246.
[30] Hecker SS, Timofeeva LF. A tale of two diagrams. In: Cooper NG, editor. Los Alamos Science, No. 26, Challenges in Plutonium Science, Los Alamos, Los Alamos National Laboratory; 2000, p. 244-251.

[31] Baskes MI, Muralidharan K, Stan M, Valone SM, Cherne FJ. Using the modified embedded-atom method to calculate the properties of Pu–Ga alloys. JOM 2003;55(9):41-50.
[32] Turchi PEA, Kaufman L, Liu Z-K, Zhou S. Thermodynamics and kinetics of phase transformations in plutonium alloys – part 1. UCRL-TR-206658 2004.
[33] Turchi PEA, Kaufman L, Zhou S, Liu ZK. Thermostatics and kinetics of transformations in Pu-based alloys. J Alloys Comp 2007;444-445:28-35.
[34] Massalski TB, Schwartz AJ, Connections between the Pu–Ga phase diagram in the Pu-rich region and the low temperature phase transformations J Alloys Comp 2007; 444-445;98-103.
[35] Abriata JP, Laughlin DE. The third law of thermodynamics and low temperature phase stability. Prog Mat Sci 2004;49:367-387.
[36] Blobaum KJM, Krenn CR, Wall MA, Massalski TB, Schwartz AJ. Nucleation and growth of the α′ martensitic phase in Pu–Ga alloys. Acta Mat 2006;54:4001-4011.
[37] Christian JW. The theory of transformations in metals and alloys. Oxford: Pergamon Press Ltd; 1965.
[38] Laughlin DE, Jones NJ, Schwartz AJ, Massalski TB. Thermally activated martensite: Its Relationship to non-thermally activated (athermal) martensite. In: Proceedings of the International Conference on Martensitic Transformations, June 29-July 5, 2008, Santa Fe, NM USA.
[39] Orme JT, Faiers ME, Ward BJ. The kinetics of the delta to alpha transformation in Pu rich Pu–Ga alloys. In: Blank H, Lindner R, editors. Plutonium 1975 and Other Actinides, Amsterdam: North Holland Publishing Co; 1975, p. 761-773.
[40] Goldberg A, Massalski TB. Phase transformations in the actinides. In: Miner WN, editor. Plutonium 1970 and Other Actinides, New York: The Metallurgical Society of AIME; 1970, p. 875-973.
[41] Hecker SS, Harbur DR, Zocco TG. Phase stability and phase transformations in Pu–Ga alloys. Prog Mat Sci 2004;49:429-485.
[42] Schwartz AJ. Plutonium metallurgy: the materials science challenges bridging condensed-matter physics and chemistry. J Alloys Comp 2007;444-445:4-10.
[43] Harbur DR. The effect of pressure on phase-stability in the Pu–Ga alloy system. J Alloys Comp 2007;444-445:249-256.
[44] Elliott RO, Olsen CE, Louie J. Electrical behavior below 300 °K of plutonium-rich, delta-phase solid solution alloys containing cerium, aluminum and zinc. J Phys Chem Solids 1962;23:1029-1044.
[45] Joel J, Roux C, Rapin M. Resistivite electrique des solutions solides d'alliages Pu–Ga en phase δ a tres basses temperatures (4.2–300K) J Nucl Mater 1971;40:297-304.
[46] Faiers ME, Loasby RG, Ward BJ, Orme JT, Spicer BR. Transformation kinetics of the α-β and δ-α transitions in pure and alloyed plutonium. In: Kay AE, Waldron MB, editors. Third International Conference on Plutonium, (also called Plutonium 1965), London; Chapman and Hall; 1967, p. 64-87.
[47] Hecker, SS, Zukas EG, Morgan JR, Pereyra RA. Temperature-induced transformations in a Pu – 2.0 at.% Al alloy. In: Aaronson HL, Laughlin DE, Sekerka RF, Wayman CM, editors. Proceedings of an international conference on

solid → solid phase transformations, Warrendale: The Metallurgical Society of AIME; 1982, p. 1339-1343.
[48] Zocco TG, Stevens MF, Adler PH, Sheldon RI, Olson GB. Crystallography of the δ → α phase transformation in a Pu–Ga alloy. Acta Metall Mater 1990;38(11):2275-2282.
[49] Deloffre P. An analysis of the stability of the δ phase of plutonium alloys obtained by the addition of deltagenic elements. Doctor of Sciences Dissertation from the University of Paris-South, Scientific Training and Research Unit (U.F.R.), Orsay, 1997.
[50] Deloffre P, Truffier JL, Falanga A. Phase transformation in Pu–Ga alloys at low temperature and under pressure: limit stability of the δ phase. J Alloys Comp 1998;271-273:370-73.
[51] Mitchell JN, Stan M, Schwartz DS, Boehlert CJ. Phase stability and phase transformations in plutonium and plutonium-gallium alloys. Met Mat Trans 2004;35A:2267-2278.
[52] Blobaum KJM, Krenn CR, Mitchell JN, Haslam JJ, Wall MA, Massalski TB, Schwartz AJ. Evidence of transformation bursts during thermal cycling of a Pu–Ga alloy. Met Mat Trans 2006;37A:567-577.
[53] Moore KT, Krenn CR, Wall MA, Schwartz AJ. Orientation relationship, habit plan, twin relationship, interfacial structure, and plastic deformation resulting from the δ → α′ isothermal martensitic transformation in Pu–Ga alloys. Met and Mat Trans 2007;38A:212-222.
[54] Oudot B, Ph.D. dissertation, "Étude de l′auto-irradiateion des alliages de plutonium," L′UFR Des Sciences et Techniques de L′Universite De Franche Comte, 2005.
[55] Oudot B, Blobaum KJM, Wall MA, Schwartz AJ. Supporting evidence for double-C curve kinetics in the isothermal δ → α′ phase transformation in a Pu–Ga alloy. J Alloys Comp 2007; 444-445:230-235.
[56] Hambling, PG, Spicer BR, White JS. The effect of uniaxial compression upon the transformation of metastable delta-phase plutonium. J Nucl Mater 1965;17:172-8.
[57] Goldberg A, Rose RL, Shyne JC. Effect of stress and plastic deformation on the transformation of the delta phase in a Pu – 1 at.% Ga alloy. J Nucl Mater 1975;55:33-52.
[58] Goldberg A, Shyne JC. Thermodynamic analysis of stress and pressure effects on the δ → α transformation in plutonium alloys. J Nucl Mater 1976;60:137-144.
[59] Zukas EG, Hecker SS, Morgan JR, Pereyra RA. Pressure-induced transformation in a Pu – 2.0 at.% Al alloy. In: Aaronson HL, Laughlin DE, Sekerka RF, Wayman CM, editors. Proceedings of an international conference on Solid → Solid phase transformations, Warrendale: The Metallurgical Society of AIME; 1982, p. 1339-1343.
[60] Faure Ph, Klosek V, Genestier C, Baclet N, Heathman S, Normile P, Haire R. Structural investigation of δ-stabilized plutonium alloys under pressure. In: Sarrao JL, Schwartz AJ, Burns PC, Haire RG, Nitche H. editors. Actinides 2005 – Basic Science, Applications and Technology, Materials Research Society Proceedings, 893, Pittsburgh: Materials Research Society; 2006, p. 223-232.

[61] Adler, PH, Olson GB. Thermodynamics and kinetics of δ → α martensitic transformation in Pu Alloys. Met Trans 1988;19A:2705-2711.
[62] Elliott RO, Gschneider Jr KA, Kemmpter CP. Thermal expansion and some delta plutonium split solution alloys. In: Grison E, Lord WBH, Fowler RD. Plutonium 1960, London; Cleaver-Hume Press Ltd. 1961, p. 142-154.
[63] Hirth JP, Mitchell JN, Schwartz DS, Mitchell TE. On the fcc → monoclinic martensite transformation in a Pu – 1.7 at.% Ga alloy. Acta Mat 2006;54:1917-1925.
[64] Krenn CR, Wall MA, Schwartz AJ. Transformation crystallography and plasticity of the delta to alpha-prime transformation on plutonium alloys. In: Soderholm L, Joyce JJ, Nicol MF, Shuh DK, Tobin JG, editors. Actinides—Basic Science, Applications, and Technology, Pittsburgh; Materials Research Society; vol. 802, 2004, p. 9-14.
[65] Lomer WM. The α → δ transformation in plutonium. Solid State Communications 1963;1:96-8.
[66] Choudhry MA, Crocker AG. The crystallography of the δ to α martensitic transformation in plutonium alloys. J Nucl Mater 1985;127:119-124.
[67] Olson GB, Adler PH. On the lattice correspondence of the delta → alpha displacive transformation in plutonium alloys. Scripta Met 1984;18(4):401-6.
[68] Adler PH, Olson GB, Margolies DS. Kinematics of δ → α and α → δ martensitic transformation in plutonium alloys. Acta Met 1986;34(10):2053-2064.
[69] Jin YM, Wang YU, Khachaturyan AG, Krenn CR, Schwartz AJ. Crystallography of the δ → α martensitic transformation in plutonium alloys. Met Mat Trans 2005;36A:2031-2047.
[70] Massalski TB. Massive transformations. Mat Sci Engr 1976;25:119-125.
[71] Jeffries JR, Blobaum KJM, Wall MA, Schwartz AJ. Enabling the Double-C Curve in Pu–Ga Alloy Time-Temperature-Transformation Diagrams. In: Chung B, Albrecht-Schmitt T, Gouder T, Shuh D, Thompson J, editors. Actinides IV – Basic Science, Applications and Technology, Materials Research Society Proceedings, 1104, Pittsburgh: Materials Research Society; 2008, p. 31-36.
[72] Sadigh B, Wolfer WG. Gallium stabilization of δ-Pu: Density-functional calculations. Phys Rev B 2005;72:205122.
[73] Nelson EJ, Blobaum KJM, Wall MA, Allen PG, Schwartz AJ, Booth CH. Local structure and vibrational properties of α′-Pu martensite in Ga-stabilized δ-Pu. Phys Rev B 2003;67:224206.
[74] Imai Y, Izumiyama M, Sasaki K. Isothermal martensitic transformation in Fe–Ni–Cr alloy. Science reports of the Research Institutes Tohoku University Series A-Physics Chemistry and Metallurgy 1966;18(1):39-48.
[75] Lookman T, Saxena A, Albers RC. Phonon mechanisms and transformation paths in Pu. Phys Rev Lett 2008;100:145504.
[76] Jeffries JR, Blobaum KJM, Wall MA, Schwartz AJ. Ambient-temperature Conditioning as a Probe of Double-C Transformation Mechanisms in Pu – 2.0 at.% Ga. In: Chung B, Albrecht-Schmitt T, Gouder T, Shuh D, Thompson J, editors. Actinides IV – Basic Science, Applications and Technology, Materials Research Society Proceedings, 1104, Pittsburgh: Materials Research Society; 2008, p. 25-30.

[77] Migliori A, Mihut I, Betts JB, Ramos M, Mielke C, et al. Temperature and time-dependence of the elastic moduli of Pu and Pu–Ga alloys. J Acoustic Soc Am 2007;122(4):1994-2001.
[78] Hecker SS. The complex world of plutonium science. MRS Bulletin 2001;26(9):672-8.
[79] Zachariasen WH, Ellinger F. The crystal structure of alpha-plutonium metal. J Chem Phys 1957;27(3):811-812.
[80] Zachariasen WH, Ellinger FH. The crystal structure of alpha plutonium metal. Acta Cryst 1963;16:777-783.
[81] Dewaele A, Loubeyre P, Mezouar M. Equations of state of six metals above 94 GPa. Phys Rev B 2004;70(9):094112.
[82] Moore KT, Wall MA, Schwartz AJ. Experimental verification of the existence and structure of z Pu_6Fe in a Pu–Ga alloy. J Nucl Mater 2002;306:213-7.
[83] Arko AJ, Joyce, JJ, Morales L, Wills, Lashley J. Electronic structure of α- and δ-Pu from photoelectron spectroscopy. Phys Rev B 2000;62(3):1773-9.
[84] Lashley JC, Lawson A, McQueeney RJ, Lander GH. Absence of magnetic moments in plutonium. Phys Rev B 2005;72:054416.
[85] Tobin JG, Moore KT, Chung BW, Wall MA, Schwartz AJ, van der Laan G, Kutepov AL. Competition between delocalization and spin-orbit splitting in the actinide *5f* states. Phys Rev B 2005;72:085109.
[86] Javorsky P, Havela L, Wastin F, Colineau E, Bouëxiere D. Specific Heat of δ-Pu stabilized by Am. Phys Rev Lett 2006;96:156404.
[87] Moore KT, van der Laan G, Haire RG, Wall MA, Schwartz AJ. Oxidation and aging in U and Pu probed by spin-orbit sum rule analysis: Indications for covalent metal-oxide bonds. Phys Rev B 2006;73:033109.
[88] Moore KT, van der Laan G, Wall MA, Schwartz AJ, Haire RG. Rampant changes in $5f_{5/2}$ and $5f_{7/2}$ filling across the light and middle actinide metals: Electron energy-loss spectroscopy, many-electron atomic spectral calculations and spin-orbit sum rule. Phys Rev B 2007;76:073105.
[89] Moore KT, van der Laan G, Haire RG, Wall MA, Schwartz AJ, Söderlind P. Emergence of strong exchange interaction in the actinide series: the driving force for magnetic stabilization of curium. Phys Rev Lett. 2007;98:236402.
[90] Butterfield MT, Moore KT, van der Laan G, Wall MA, Haire RG. Understanding the $O_{4,5}$ edge structure of actinide metals: Electron energy-loss spectroscopy and atomic spectral calculations of Th, U, Np, Pu, Am, and Cm. Phys Rev B 2008;77:113109.
[91] Wills JM, Eriksson O, Delin A, Andersson PH, Joyce JJ, et al. A novel electronic configuration of the 5f states in δ-plutonium as revealed by the photo-electron spectra. J Elec. Spect and Related Phenomena 2004;135:163-166.
[92] Shim JH, Haule K, Kotliar G. Fluctuating valence in a correlated solid and the anomalous properties of δ-plutonium. Nature 2007;446:513-516.
[93] Moore KT. Wall MA, Schwartz AJ, Chung BW, Morton SA, Tobin JG, et al. Electron-energy-loss spectroscopy and x-ray absorption spectroscopy as complementary probes for complex f-electron metals: cerium and plutonium. Phil Mag 2004;84(10):1039-1056.

[94] Zhu J-X, McMahan AK, Jones MD, Durakiewicz T, Joyce JJ, Wills JM, Albers RC. Spectral properties of δ-plutonium: Sensitivity to 5*f* occupancy. Phys Rev B 2007;76:245118.
[95] Dai X, Savrasov SY, Kotliar G, Migliori A, Ledbetter H, Abrahams E. Calculated phonon spectra of plutonium at high temperatures. Science 2003;300:953-5.
[96] Wong J, Krisch, M, Farber DL, Occelli F, Schwartz AJ, Chiang TC, et al. Phonon dispersions of fcc δ-plutonium-gallium by inelastic x-ray scattering. Science. 2003;301:1078-1080.
[97] Wong J, Krisch, M, Farber DL, Occelli F, Xu R, Chiang TC, et al. Crystal dynamics of δ fcc Pu–Ga alloy by high-resolution inelastic x-ray scattering. Phys Rev B 2005;72:064115.
[98] Baskes MI. Atomistic model of plutonium. Phys Rev B 2000;62(23):15532-7.
[99] Baskes MI, Lawson AC, Valone SM. Lattice vibrations in δ-plutonium: Molecular dynamics calculations. Phys Rev B 2005;72:014129.
[100] Lawson, AC, Martinez B, Von Dreele RB, Roberts JA, Sheldon RI, Brun TO, Richardson Jr JW. Vibrational order in $Pu_{0.98}Ga_{0.02}$. Phil Mag B 2000;80(11):1869-1891.
[101] Lawson AC, Roberts JA, Martinez B, Von Dreele RB, Storey B, Hawkins HT, et al. Lattice constants and anisotropic microstrain at low temperature in ^{242}Pu–Ga alloys. Phil Mag 2005;85(18):2007-2022.
[102] Cox LE, Martinez R, Nickel JH, Conradson SD, Allen PG. Short-range atomic structure of 1 wt.% Ga δ-stabilized plutonium by x-ray absorption fine-structure spectroscopy. Phys Rev B 1995;51(2):751-5
[103] Alexander CA, Wood VE. Thermal conductivity of plutonium above room temperature. J Appl Phys 2008;103:063704.
[104] Ahuja R., Söderlind P, Trygg J, Melsen J, Wills JM, Johansson B, Eriksson O. Influence of pseudocore valence-band hybridization on the crystal-structure phase stabilities of transition metals under extreme compressions. Phys Rev B 1994;50:14690-93.
[105] Söderlind P. Theory of the crystal structures of cerium and the light actinides. Adv. Phys 1998;47(6):959-998.
[106] Moore KT, Söderlind P, Schwartz AJ, Laughlin DE. Symmetry and stability of δ plutonium: The influence of electronic structure. Phys Rev Lett 2006;96:206402.
[107] Moore KT, Laughlin DE, Söderlind P, Schwartz AJ. Incorporating anisotropic electronic structure in crystallographic determination of complex metals: iron and plutonium. Phil Mag 2007;87(17):2571-2588.
[108] Wills JM, Eriksson O, Alouani M, Price DL. The Uses of the LMTO Method. In: Dreysse H, editor. Electronic Structure and Physical Properties of Solids. Berlin: Springer-Verlag; 2000, p. 148-167.
[109] Perdew JP, Chevary JA, Vosko SH, Jackson KA, Pederson MR, Singh DJ. Atoms, molecules, solids, and surfaces: Applications of the generalized gradient approximation for exchange and correlation. Phys Rev B 1992;46(11):6671-87.
[110] Faure Ph, Deslandes B, Bazin D, Tailland C, Doukhan R, Fournier JM, Falanga A. Lattice collapse around gallium in PuGa alloys as revealed by x-ray absorption spectroscopy. J Alloy Comp 1996;244:131-9.

[111] Baskes MI, Hu SY, Valone SM, Wang GF, Lawson AC. Atomistic simulations of Ga atom ordering in Pu 5 at.% Ga alloys. J Computer-Aided Mater Des 2007;14:379-388.
[112] Dremov V, Sapozhnikov P, Kutepov, A, Anisimov V, Korotin M, et al. Atomistic simulations of helium dynamics in a plutonium lattice. Phys Rev B 2008;77:224306.

Figure Captions

Fig. 1. Proposed phase diagrams of Pu alloys with Al, Ga, In, and Tl (reproduced from [26]) illustrating the influence of alloying element on δ phase stability. Although the details of phase diagram above the δ phase are unclear, the sequence of diagrams demonstrates the trend in the eutectoid temperature with alloying element.

Fig. 2. Pu–Ga phase diagrams. (a) Equilibrium phase diagram with modifications to the diagram published by Hecker and Timofeeva [30], and (b) "Working" phase diagram based on the original work by Ellinger [20].

Fig. 3. Calculated $T_o^{\delta/\alpha}$ temperature for the equivalence of free energies between the α and δ phases [29, 32-34]. Also included are the martensite start (δ → α′) and reversion start (α′ → δ) temperatures as a function of Ga content. Note that this is the 5% transformation curve.

Fig. 4. Optical micrograph of a Pu – 2 at.% Ga alloy, annealed at 375 °C for 8 hours, "conditioned" at 25 °C for 8 hours, and then quenched to –155 °C and held for 4 hours. The α′ particles are the high aspect ratio shapes with light contrast. The δ matrix exhibits dark contrast.

Fig. 5. TEM images and diffraction pattern of the α′ particles in the δ matrix. (a) Bright-field image (b) electron diffraction pattern from the two-phase region, and (c) high-resolution image.

Fig 6. Time-Temperature-Transformation diagram for a Pu – 1.9 at.% Ga alloy (adapted from [39]).

Fig. 7. Differential scanning calorimetry scans (at 20 °C/min) of a Pu – 2.0 at.% Ga alloy that was conditioned at 25 °C for 0 – 12 hours. Peak areas for both the δ → α′ transformation on cooling (a) and the α′ → δ reversion on heating (b) increase as the conditioning time increases, with a plateau at approximately 6 hours.

Fig. 8. The amount of δ → α′ transformation on cooling as a function of conditioning time at 25 °C. The amount of transformation product increases rapidly as a result of the first 4 hours of conditioning. No additional transformation on cooling is observed for conditioning treatments of 6 hours or longer.

Fig. 9. Differential scanning calorimetry scans (at 20 °C/min) of a Pu – 2.0 at.% Ga alloy that was conditioned at temperatures between -50 °C and 370 °C. (a) Cooling curve and (b) heating curve. The largest amount of α′ is formed when the sampled is conditioned for 12 hours at 25 °C.

Fig. 10. Differential scanning calorimetry scans (heating at 20 °C/min) of the α′ → δ reversion in a well-homogenized Pu – 2.0 at.% Ga alloy. Prior to the δ → α′ transformation on cooling (not shown), the sample was annealed at 375 °C for 8 hours and then conditioned at the temperatures indicated on the graph for 8 hours.

Fig. 11. (a) Cooling portion of DSC scans from a partially homogenized Pu – 2.0 at.% Ga alloy. The exothermic peaks correspond to the δ → α′ martensitic transformation. M_s is the martensite start temperature. (b) Heating portion of DSC scans from a partially homogenized Pu – 2.0 at.% Ga alloy. The endothermic peaks correspond to the cooperative α′ → δ reversion. Sharp spikes are evident on the high-temperature side of the 20 °C/min scan, and throughout the 1.5 °C/min scan.

Fig. 12. Heating portion (at 20 °C/min) of a DSC scan from a well-homogenized Pu – 2.0 at.% Ga alloy. Sharp spikes are evident on the high-temperature side of the endothermic α′ → δ reversion peak.

Fig. 13. Differential scanning calorimetry trace showing the isothermal α′ → δ reversion at 65 °C in a partially homogenized Pu – 2.0 at.% Ga alloy.

Fig. 14. (a) Isothermal holds at temperatures between 65 °C and 105 °C. The Pu – 2.0 at.% Ga sample was cooled to form α′, heated at 20 °C/min to 65 °C and held for 45 minutes. Following the initial isothermal hold, the temperature was increased in 5 °C increments, with a 45 minute hold at each temperature. Although there is significant noise in the data, some sharp spikes corresponding to the cooperative $\alpha' \rightarrow \delta$ reversion are evident, particularly at 65 °C, 90 °C, and 105 °C. It is interesting to note that the largest spike at 90 °C occurs after an incubation time of 15 minutes at this temperature. (b) Following the stepped isothermal holds shown in Fig. 14a, the sample was heated at 20 °C/min to complete the $\alpha' \rightarrow \delta$ reversion. This isochronal scan shows multiple cooperative bursts that extend to temperatures significantly higher than observed when the sample is not held isothermally during the reversion.

Fig. 15. Isochronal heating scans at 10 °C/min and 20 °C/min showing the range of temperatures over which the $\alpha' \rightarrow \delta$ reversion occurs (25 °C to 127 °C).

Fig. 16. Intensity versus 2Θ plots showing pressure-induced transformations of δ-Pu (Pu – 3.3 at.% Ga) up to 1.95 GPa. The initial δ-phase sample transforms to a mixture of α′ and γ′, finally transforming to 100% α′ at 1.95 GPa, the highest pressure of these studies. Very weak α′ peaks can be seen at the lowest pressure. These weak peaks are likely a result of pressure-induced transformations caused during the sample preparation (mechanical deformation due to cutting).

Fig. 17. A plot of volume versus pressure, showing the pressure-induced progression through the δ (δ′), γ′ and α′ phases. The δ (δ′), γ′ and α′ phases are shown as open circles squares, and triangle, respectively. A line is drawn through each phase as a guide. There is a broad coexistence regime between 0.6 and 1.35 GPa.

Fig. 18. Comparison of representative plots of the δ and δ′ phases at very low pressure (~0 GPa). The lower trace shows a δ-Pu XRD pattern with indexing of diffraction peaks noted. The upper trace shows a δ′-Pu XRD pattern with peak splitting, manifested as line broadening, which is indexed as a body-centered-tetragonal crystal structure.

Fig. 19. Photograph of large volume moissanite anvil cell used for compressing TEM-sized samples.

Fig. 20. X-ray diffraction pattern taken from a Pu – 2.0 at.% Ga sample that was compressed to 1 GPa and characterized at ambient pressure. Strong α′ peaks and weak δ peaks are evident.

Fig. 21. Bright-field TEM image of a Pu – 2.0 at.% Ga sample that was compressed to 1 GPa and characterized at ambient pressure. The insert shows an electron diffraction pattern from a neighboring area that reveals Bragg peaks from both the α′ and δ phases.

Fig. 22. Two stacked fcc unit cells with the central atom showing the 12 nearest neighbors. In the case of plutonium, the 12 bonds with the nearest neighbors vary widely in strength and can be separated into six pairs: blue (3.3), black (3.5-3.7), red (3.7-3.9), pink (3.9-4.1), green (4.5-4.7), and brown (4.7-5.3). When the fcc lattice is combined with the motif of these bond strengths the resultant space group is monoclinic *Cm*. The bond strengths as calculated with density-functional theory of the twelve nearest neighbors can be separated into six pairs of two where the bond strengths are close in value: blue (3.3), black (3.5-3.7), red (3.7-3.9), pink (3.9-4.1), green (4.5-4.7), and brown (4.7-5.3). In the (001) plane, the [110] bond is roughly equal to the $[\bar{1}\bar{1}0]$ bond (green), and the $[\bar{1}10]$ bond is roughly equal to the $[1\bar{1}0]$ bond (black). In the {011} planes, however, we see that $[0\bar{1}1]$~$[\bar{1}0\bar{1}]$ (blue), $[0\bar{1}\bar{1}]$~$[10\bar{1}]$ (red), $[0\bar{1}1]$~[101] (pink), and [011]~$[\bar{1}01]$ (brown).

Fig. 23. The Bravais lattice of the *c*-centered monoclinic unit cell. (a) The three-dimensional rendering of the *c*-centered unit cell and (b) a two-dimensional rendering viewed along the [001] direction where the fcc

lattice is shown by the purple box. The *c*-centered unit cell is shown by the heavy red box with the green line marking the [110] mirror plane.

Table captions

Table 1
Percentages of α′, δ, and amorphous phases after compression to 1 GPa and release to ambient pressure for three different alloys [43].

Table 2
The nearest neighbor direction in *x*, *y*, *z* coordinates, Miller indices (*h k l*), and bond strength *F* (mRy/Å) for pure Pu and a gallium atom in a Pu – 3.7 at.% Ga alloy.